AD 269 504

ARF

ARF 1139 - 11
FINAL REPORT

ARMOUR RESEARCH FOUNDATION OF ILLINOIS INSTITUTE OF TECHNOLOGY

INFRARED FIBER OPTICS

Commander
Wright Air Development Division
Wright-Patterson Air Force Base
Dayton, Ohio

Contract No. AF 33(616)-6247

25 years of research ARF

ARMOUR RESEARCH FOUNDATION OF ILLINOIS INSTITUTE OF TECHNOLOGY

ARF 1139-11

FINAL REPORT

INFRARED FIBER OPTICS

to

Commander
Wright Air Development Division
Wright-Patterson Air Force Base
Dayton, Ohio

Contract No. AF (616)-6247

(Covering the period from March 1, 1960 to September 30, 1961.)

Submitted by:

ARMOUR RESEARCH FOUNDATION
of Illinois Institute of Technology
Chicago 16, Illinois

December 14, 1961

DISTRIBUTION LIST

ARF 1139-11 Final Report, Contract AF 33(616)-6247

Copy No.	Recipient
1-7	Commander Wright Air Development Division Wright-Patterson Air Force Base, Ohio
1-2	Attn: WCLGDPI, Mr. T. L. Durgans
3	Attn: WCLGSFA, Mr. L. J. Pleshek
4	Attn: WCLGGEH, Mr. W. P. Kennedy
5	Attn: WCLDGLA, Mr. V. G. Lager
6	Attn: WCOSI-3, (Library).
7	WCLGDPL, Mr. R. Lower
8-10	Air Technical Intelligence Center Wright-Patterson Air Force Base, Ohio Attn: AFCIN-4A1B, Dr. Paul Overbo Attn: AFCIN-4E1D, Mr. Bisson Attn: AFCIN-4A1B, Mr. Meeker
11-14	Directorate of Systems Management Air Research and Development Command Wright-Patterson Air Force Base, Ohio Attn: RDZSDG, Maj. F. Augustyne Attn: RDZSTD, Mr. J. Singer Attn: RDZSSL, Mr. W. Grimes Attn: RDZSSE, Maj. D. Ingram
15	Headquarters Air Research and Development Command Andrews Air Force Base Washington 25, D. C. Attn: RDTCEA, Capt. J. Stevens
16	U. S. Army Guided Missile Agency Redstone Arsenal Huntsville, Alabama Attn: ORDXR-REE, PFC. P. Birman
17	Commanding Officer Evans Signal Laboratory Fort Monmouth, New Jersey Attn: Mr. Harry Dauber

DISTRIBUTION LIST (continued)

Copy No.	Recipient
18	Rand Corporation 1700 Main Street Santa Monica, California Attn: Dr. Sidney Passman
19	Chief, Bureau of Aeronautics Department of the Navy Attn: Aer-SC-41 Washington 25, D. C.
20-22	Chief, Bureau of Ordnance Department of the Navy Washington 25, D. C. Attn: ReO Attn: ReW1 Attn: Re02
23	Commander U. S. Naval Ordnance Test Station China Lake, California Attn: Code 4052
24	Chief, Bureau of Aeronautics Attn: AV and GM Divisions Department of the Navy Washington 25, D. C.
25	General Electric Company Advanced Electronics Center Tomplins County Airport Ithaca, New York Attn: Mr. Charles V. Townsend
26	Avion Division ACF Industries, Inc. Paramus, New Jersey Attn: Mr. Harvey Dubner

DISTRIBUTION LIST(Continued)

Copy No.	Recipient
27	Boeing Airplane Company, Bomarc Weapons Systems Project Office Seattle, Washington Attn: Mr. R. R. Barber, Head Librarian
28	Sylvania Electric Products, Inc. Waltham Laboratory Library Waltham, Massachusetts Attn: Mr. C. Thornhill VIA: Boston Ordnance District Boston Army Base Boston 10, Massachusetts Attn: Mr. E. J. Donovan
29	Eastman Kodak Company Apparatus and Optical Division 121 Lincoln Avenue Rochester, New York Attn: Dr. Edward McAllister (For use on Contract 33(616)-6156)
30	Director Air University Library Maxwell Air Force Base, Alabama Attn: AUL-9856
31	North American Aviation, Inc. Englewood Division B-70 Weapons Systems Project Office International Airport Los Angeles 45, California Attn: Mr. Kemp
32	Westinghouse Electric Corporation Air Armaments Division P. O. Box 746 Baltimore, Maryland Attn: Miss G. E. Lambie, Librarian

DISTRIBUTION LIST (continued)

Copy No.	Recipient
33	Santa Barbara Research Center Santa Barbara Airport Goleta, California Attn: Mr. P. M. Cruse
34	Aerojet General Corporation Avionics Division Azusa, California Attn: Mr. M. Boatwright
35-36	Commander Naval Ordnance Test Station China Lake, California Attn: Code 4050, Mr. R. G. McCarty Attn: Code 3529, Mr. E. Regelson
37	Commander Air Force Cambridge Research Center Laurence G. Hanscom Field Bedford, Massachusetts Attn: CRZCI, Dr. John Howard
38-44	Commander Armed Services Technical Information Agency Arlington Hall Station Arlington 12, Virginia Attn: TIPDR
45-46	Infrared Information and Analysis (IRIA) University of Michigan Willow Run Research Laboratories Willow Run Airport Ypsilanti, Michigan Attn: Mr. William Wolfe Attn: Mr. J. King (AF(616)-5559)

DISTRIBUTION LIST (continued)

Copy No.	Recipient
47	Dr. N. S. Kapany Optics Technology, Inc. 248 Harbor Boulevard Belmont, California
	ARF Internal Distribution:
48	Report Library via K. W. Miller.
49	Main Files
50	"A" files via L. Reiffel
51	Mr. P. H. Wyckoff, Acting Supervisor Optics Research
52-60	Optics Section Files

ABSTRACT

Vitreous infrared transmitting materials have been drawn into coated and uncoated fibers by employing techniques developed for the formation of visible radiation transmitting glass coated-glass fiber. Infrared transmitting fiber has been fabricated from germanate, silicate and arsenic trisulfide. Crystalline sodium chloride was extruded into relatively large diameter fiber. Plastic materials such as the epoxies and lucite are shown to be suitable potting materials for uncoated fiber. Absorption bands of these materials do not seriously influence the transmitted radiation, however, compounds having few absorption bands are to be favored. The performance of fibers of diameter comparable to the wavelength of the transmitted radiation is analyzed by using dielectric waveguide theory, and the results are interpreted from the optical viewpoint of thin film interference and frustrated total reflection. Experimental measurements of the fiber spread function are made for assemblies of close-packed fibers, and its dependence on fiber diameter, spacing, wavelength and indicies of refraction is investigated.

TABLE OF CONTENTS

	Page No.
ABSTRACT	vii
List of Figures	ix
List of Tables	x
I. INTRODUCTION	1
II. INFRARED FIBER MATERIALS	2
A. Arsenic Trisulfide Fiber.	4
B. Silver Chloride Fiber.	8
C. Magnesium Oxide Fiber.	10
D. Potting of Fiber.	12
III. CONE CONDENSER	14
IV. TRANSMISSION OF FIBER BUNDLES	15
A. Instrument Design.	15
B. Transmission Measurements.	18
V. ENERGY TRANSFER IN SMALL DIAMETER FIBER	18
VI. CONCLUSION	27
VII. LOG BOOKS AND CONTRIBUTING PERSONNEL	30
APPENDIX A. WAVEGUIDE EFFECTS.	

LIST OF FIGURES

Figure No.		Page No.
1	Arsenic Trisulfide Fiber Cross Section.	7
2	Surface of 0.010 inch Diameter Silver Chloride Fiber.	9
3	Surface of Magnesium Oxide Fiber.	11
4	Infrared Transmission of Potting Materials.	13
5	Fiber Bundle Transmission Measurement System.	16
6	Transmission of Infrared Fiber Optics.	19
7	Apparatus for Studying Small Diameter Fiber Systems.	25

LIST OF TABLES

Table No.		Page No.
I	Infrared Transmitting Materials for Use in Fiber Optics.	3
II	Infrared Transmitting Fiber Core and Coating Combinations.	5

I. INTRODUCTION

Research in Fiber Optics for the visible region of the spectrum has been pursued along many avenues. A result of this work is the perfection of the techniques of drawing "glass-coated glass fibers" which provided fibers practically free of any surface losses on total reflection and permitted the formation of closely packed fused fiber plates. Studies of frustrated total reflection and information density transmitted by an aligned assembly of coated and uncoated fibers explained the behavior of fibers when the diameters were of geometrical optical dimensions. Drawing of "multiple fibers" fused and aligned, and of diameter comparable with or smaller than the wavelength of the transmitted radiation, stimulated studies of diffraction effects to estimate the transmission efficiency, the boundary-wave penetration and the radiation pattern of fibers. Fibers made of infrared materials transmitting from 30 to 100 times the visible wavelengths provide an experimental model for which the wavelength is many times a fiber diameter of 5 - 10μ. For these dimensions substantial energy may be conducted in the region outside the core. Also, as in the visible spectral region, infrared fiber-optics can be used in space filtering systems, image dissectors, field flatteners, light funnels and conical condensers.

Work on Contract AF 33(616)-6247 has been concerned with the extension of the experimental techniques and theoretical calculations of visible fiber optics to the infrared spectral region. Areas of infrared fiber optics receiving attention during the second year of the contract are the development of techniques for the fabrication of infrared transmitting fiber optics, the determination of the fiber characteristics and the theoretical and experimental investigation of waveguide effects. Investigations have been conducted in order to determine various parameters effecting image quality and transmission of infrared fibers and fiber systems.

II. INFRARED FIBER MATERIALS

To extend the useful range of fiber optics from visible to infrared frequencies, one requires materials which are both transparent in the long wavelength spectral region and capable of being formed into fiber. Vitreous materials which have a softening point, and therefore a working range, can be drawn by conventional techniques. Uncoated fibers of vitreous arsenic trisulfide, IR-20, IR-2, and optical crown glass have been drawn in 25-100μ diameters. Crystalline materials, such as AgCl, in general cannot be drawn into fiber form since they exhibit a sharply defined melting point and do not have as broad a working range as vitreous materials.

Table I lists materials which are potentially useable for infrared fiber optics. The first six compounds are formable into fiber by drawing or extruding techniques. The last three materials are not to be used in forming fibers but as potting compounds in the formation of fiber optics plates or bundles. Their low curing temperatures, relatively low refractive indicies, chemical inertness, surface wetting properties, and grinding and polishing properties are well suited to the potting of infrared fibers.

TABLE I

INFRARED TRANSMITTING MATERIALS FOR USE IN FIBER OPTICS

MATERIAL	TRANSMISSION RANGE	REFRACTIVE INDEX	SOFTENING POINT	MELTING POINT
ARSENIC TRISULFIDE GLASS	1-13μ	2.49(3μ)	210°C	--
ARSENIC-SULFIDE GLASS	1-13μ	2.21	170°C	--
SILVER CHLORIDE	0.4 - 25μ	2.00(3μ)	--	457.7°C
BAUSCH AND LOMB IR-20; GERMANATE GLASS	0.4 - 5μ	1.82(2μ)	770°C	--
BAUSCH AND LOMB IR-2; SILICATE GLASS	0.4 - 4.5μ	1.75(2μ)	825°C	--
OPTICAL CROWN	0.35 - 2.8μ	1.51(1μ)	600°C	--
EPOXY	0.35 - 25μ	1.51(visible)	Curing Temp.=54°C	
LUCITE	0.35 - 25μ	1.49(visible)	Curing Temp.=54°C	
KEL-F	0.25 - 16.5μ	1.43	200°C	--

The techniques of drawing optical glass coated-glass fiber have been used successfully with the infrared materials to optically insulate small diameter fibers and practically eliminate surface losses on total reflection. The transmission of such fibers is limited, therefore, primarily by the transmission of the bulk materials. Combination of materials having matched softening points, working ranges, coefficients of thermal expansion, and correct ratio of indicies are listed in Table II. All the glass-glass combinations have been drawn. Lucite and epoxy potting have been successful with most of the core materials. Excessive epoxy coating of long bundles has been experienced because of capillary action between fibers. Also, silver chloride is found to be chemically reactive with some epoxies. During the last year, the major research effort in the area of fiber formation has been confined to investigations of arsenic trisulfide, silver chloride and magnesium oxide as fiber materials and the potting of coated and uncoated fiber in lucite and epoxy.

A. Arsenic Trisulfide Fibers.

Uncoated arsenic trisulfide fibers 0.002 and 0.004 inch in diameter have been drawn from material supplied by W. A. Fraser. The fibers drawn during the last year are less brittle than those previously drawn and the surface finish is of optical quality. A flexible bundle 4.5 inches long has been prepared by potting the ends of the bundle in Scotch Cast. The fibers assumed a close packed structure in this matrix material, were held firmly, and the fiber ends could be polished easily. In addition to this bundle, a second longer

TABLE II

INFRARED TRANSMITTING FIBER CORE AND COATING COMBINATIONS

CORE	COATING	CRITICAL ANGLE	NUMERICAL APERTURE
ARSENIC TRISULFIDE	ARSENIC-SULFIDE	65.9	0.98
ARSENIC TRISULFIDE	EPOXY	37.3	1.00
ARSENIC TRISULFIDE	LUCITE	36.7	1.00
ARSENIC TRISULFIDE	KEL-F	35.0	1.00
SILVER CHLORIDE	LUCITE	49.2	1.00
SILVER CHLORIDE	EPOXY	48.2	1.00
SILVER CHLORIDE	KEL-F	45.6	1.00
IR-20 GERMANATE	IR-2 SILICATE	74.2	0.50
IR-20 GERMANATE	OPTICAL CROWN	56.1	1.00
IR-2 SILICATE	OPTICAL CROWN	59.7	0.88

bundle and a fiber plate were made. Also, a light funnel composed of 0.002 inch diameter fibers has been assembled.

A low index arsenic-sulfide material (n = 2.18) has been supplied by both W.A. Fraser and Servo Corporation of America. This material of lower index than As_2S_3 is suitable for coating of the As_2S_3 core. A tube formed from the Servo material was used with a rod of As_2S_3 supplied by Fraser in an attempt to draw coated As_2S_3 fibers. The wall thickness of the tube formed by drilling, grinding, and polishing the bulk slab was too large in proportion to the core diameter. This excess glass combined with a lower softening temperature than the core resulted in most of the arsenic-sulfide material flowing off the core in the form of tubing leaving a thin coating upon the large core which was then drawn into coated fiber. A photograph of the fiber cross section is shown in Fig. 1. Owing to the limited amounts of material a very small quantity of fiber was obtained. However, the possibility of obtaining coated As_2S_3 fiber transmitting to 13μ is established.

Drawing of coated As_2S_3 from bulk material having the core fused to the coating promises to be satisfactory provided the coating can be molded to the core. Preliminary attempts to pour low index glass around a core centered in a cylinder mold indicate that a better approach is to partially fill the mold with low index material and then press the heated As_2S_3 rod down into the mold. After the glass solidifies the aluminum mold is removed by disolving it in HCl. This experiment which was to be performed with the assistance of W.A. Fraser was never completed.

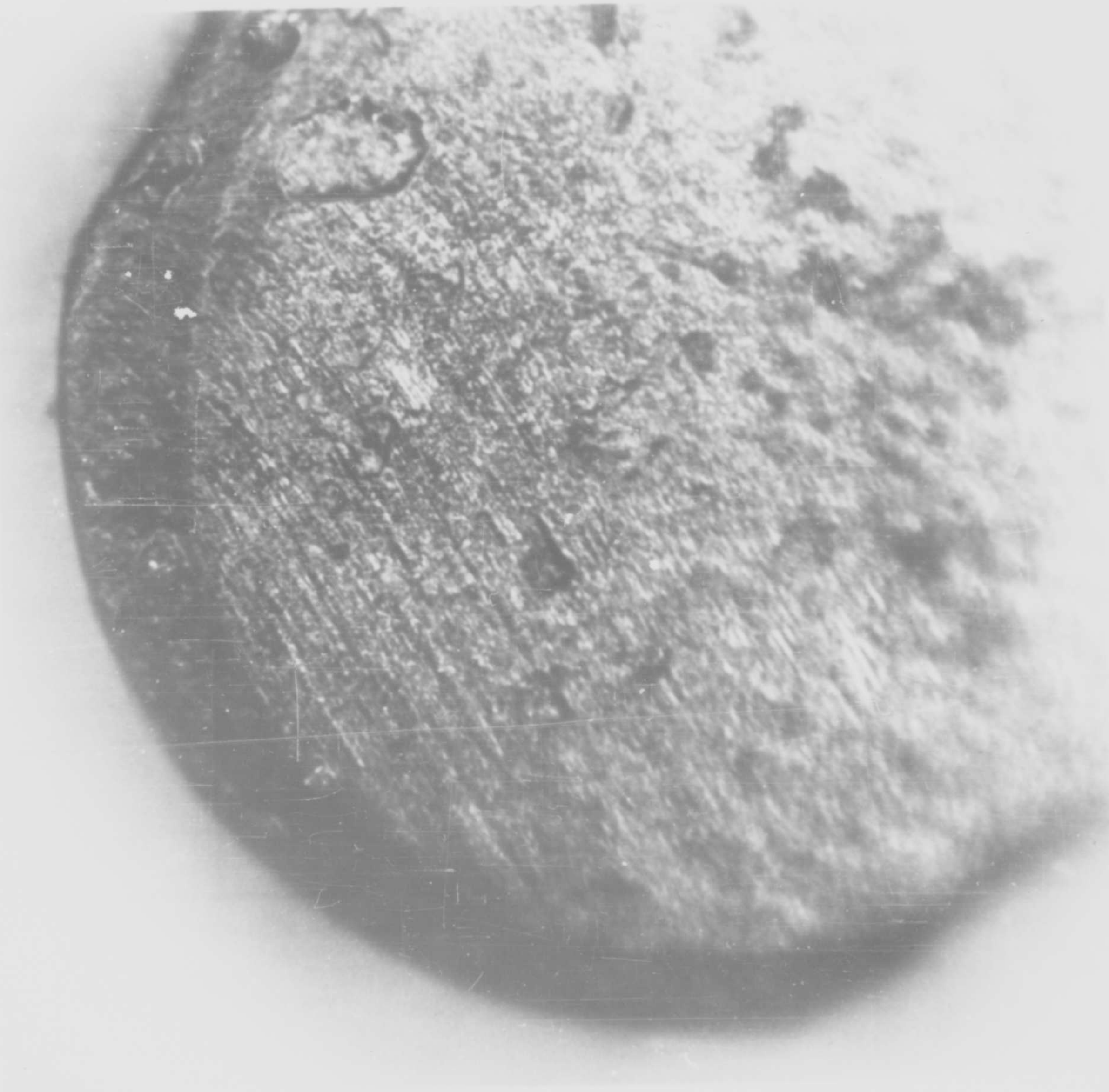

FIG. 1. ARSENIC TRISULFIDE FIBER CROSS SECTION.

B. Silver Chloride Fibers.

The transmission of infrared fibers was extended to 25μ by extruding silver chloride (AgCl) fiber. The die used for extrusion establishes the diameter and surface finish of the fiber. The surface of the die imparts its finish to the fiber, therefore, the die must be constructed of a material not corroded by AgCl at elevated temperatures and one which can be polished to optical smoothness. A silicon carbide die manufactured by Hedalloy Die Corporation was used by Harshaw Chemical Company to extrude eight feet of 0.010 inch diameter AgCl fiber. This fiber, when compared with that previously extruded during the first year of the contract, has improved surface quality but still has many imperfections as can be seen in the photomicrographs shown in Figure 2. The relatively smooth areas were probably formed during periods of uniform extrusion while the rougher areas may be attributed to discontinuous extrusion pressure. The improved surface polish of the die presently being used reduced the extrusion pressures to a level permitting the formation of 0.002-0.004 inch diameter fibers. Also, as the surface quality of the fiber did not deteriorate substantially from start to finish, it can be concluded that the die was not corroded by the AgCl.

When the lengths of silver chloride fiber shown in Figure 2 were cleaned with water and lens paper the surface finish was improved. The cleaning appeared to remove foreign matter which adhered to the fiber shortly after or during the extrusion process.

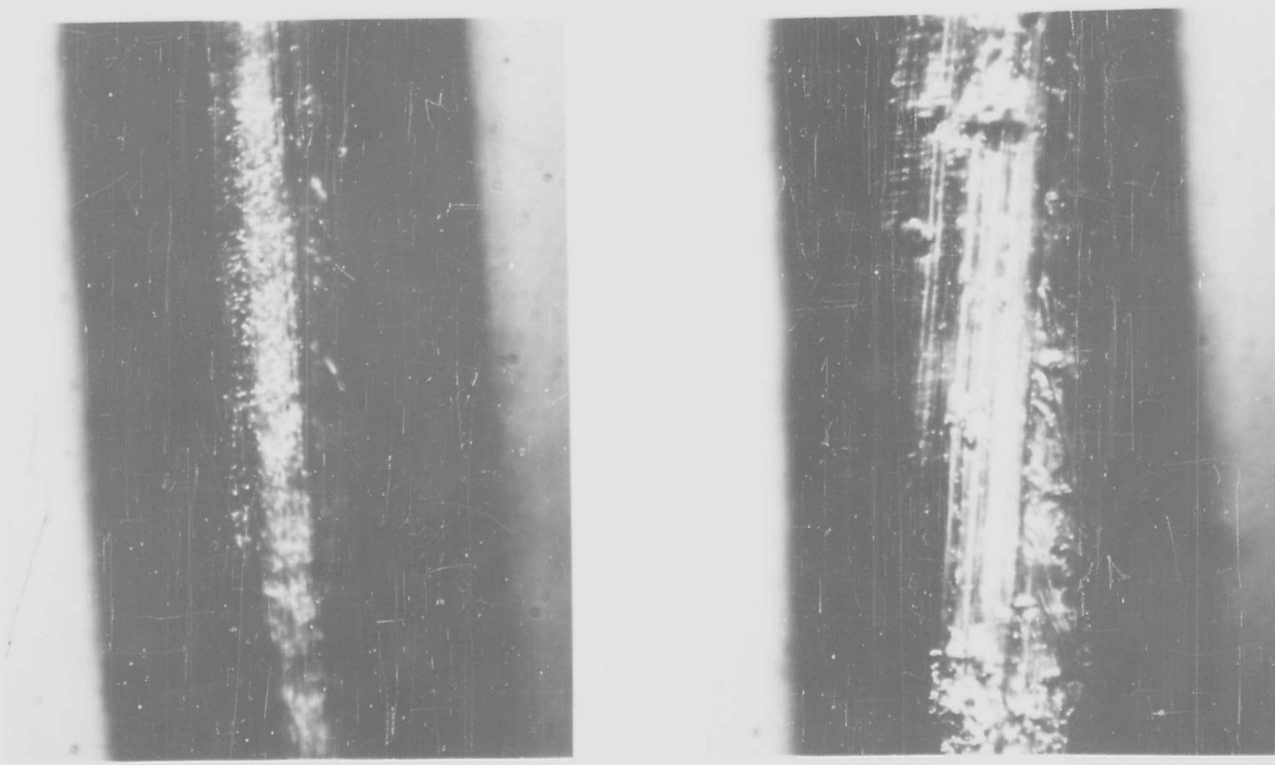

Figure 2. Surface of 0.010 inch Diameter Silver Chloride Fiber

After cleaning and assembling the di e another length of AgCl fiber was extruded from bulk material which had been carefully inspected for imperfections. Longitudinal surface scratches, possibly caused by AgCl sticking to the di e walls, which were present on fiber from the previous run were diminished in fiber from this extrusion in which the fiber was formed under uniform extrusion pressure from bulk material free of imperfections. The surface quality of this fiber is improved and the diameter of the fiber is reasonably constant; however, these fibers are not comparable in quality to glass fiber drawn from a furnace.

C. Magnesium Oxide Fiber.

A cleaved single crystal of Magnesium Oxide 1/32 x 1/32 x 1 inch was obtained from Semi-Elements, Inc. The surface of this fiber is shown in Figure 3. This fiber does not have a well polished surface but is satisfactory for applications requiring short fiber lengths. The manufacturer is able to supply MgO fibers smaller than 1/32 inch cross sections in quantities of thousands all having polished surfaces and the same dimensions. Magnesium Oxide transmits in the 0.25 - 9μ spectral region, has a refractive index of 1.66 at 4.26μ and a melting point of 2800°C. This material may be useful in applications requiring low resolution, transmission in a broad spectral band, and relatively short length fibers. The extremely high melting point precludes damage to the fiber surface by temperature effects and therefore, permits potting the fibers in nearly all known infrared materials having lower refractive indices.

Figure 3 Surface of Magnesium Oxide Fiber

D. Potting of Fibers.

In the fabrication of uncoated fibers into bundles, plates or other optical devices, a potting resin is sought which is as transparent as possible to infrared radiation in the 1 - 25μ spectral region and which will bind fibers tightly together. In addition, this plastic should not react chemically with the fiber material; it must wet the fiber surface and be sufficiently hard when set to permit grinding and polishing.

Thin layers of Kel-F, epoxy and lucite exhibit infrared absorption bands but do have extensive regions of transparency. Typical transmission curves of these three compounds are shown in Figure 4. To investigate the absorption bands our plastics group prepared samples of appropriate resins, chiefly methyl methacrylate and epoxies, for infrared transmission determination. The thin samples permit the careful location of the absorption band positions and the measurement of absorption coefficients in relatively highly absorbing materials. The samples were prepared in thicknesses of 0.010 inch deposited on the surface of sodium chloride discs. The limited experiments did not result in absorption coefficient values or in any new absorption band information. Kel-F having two absorption bands appears to be an excellent choice for a fiber bundle matrix material, but because it is highly scattering it has not been used in any applications. Thin layers of lucite transmit well in the 2-6μ and 9.5 - 15μ spectral regions. The transparent regions at 6.5 and 7.5μ may be useable for narrow spectral band width applications. Epoxylite transmits in the 2 - 6μ region except for an absorption band at

FIG. 4. INFRARED TRANSMISSION OF POTTING MATERIALS

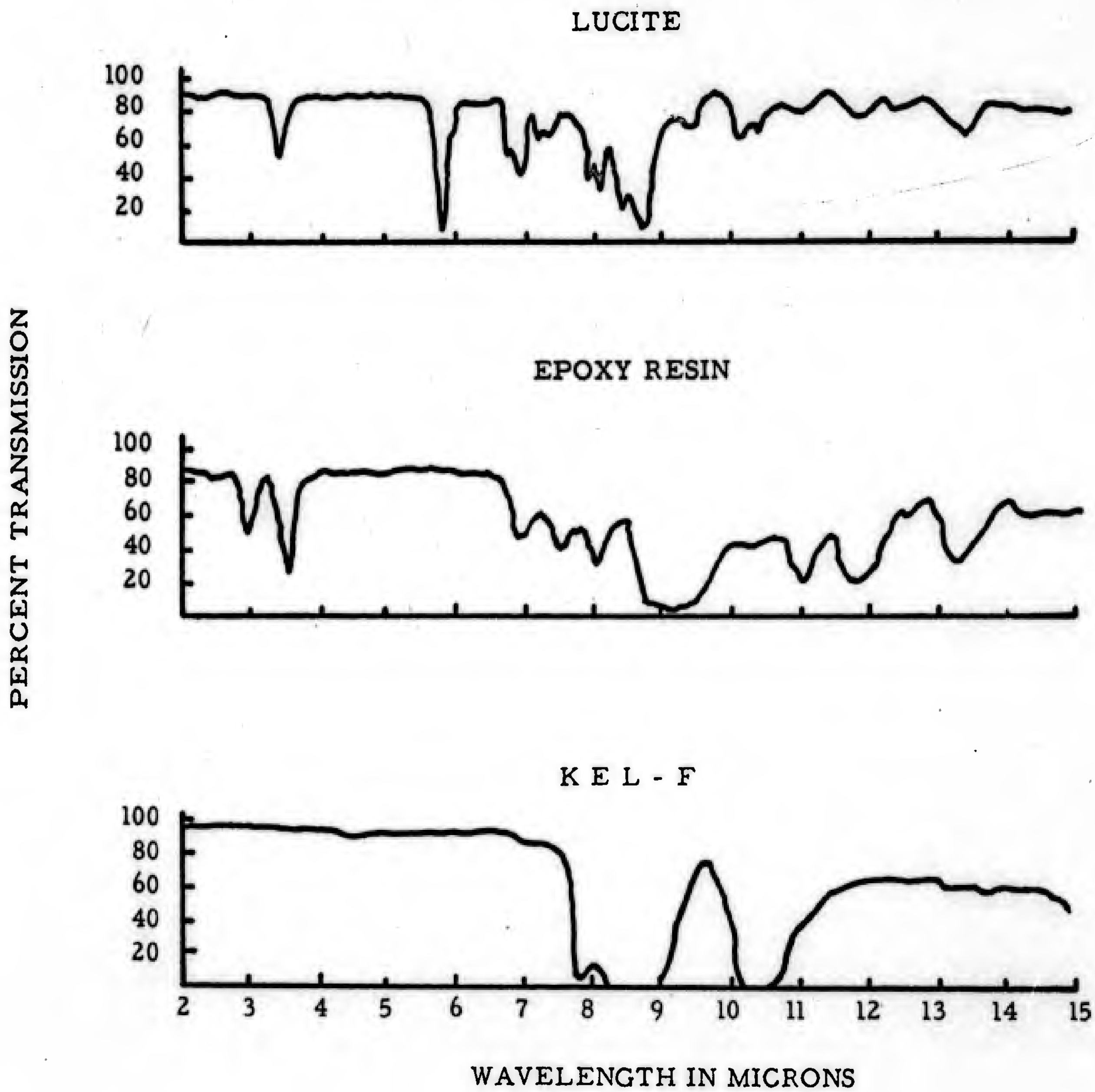

3 - 3.5μ. This material has not been obtained in thin enough samples to measure the transmission beyond 6μ, however, epoxy resins transmit beyond 10.0μ up to 15μ and may be suitable for infrared fibers having long wavelength transmission.

The absorption bands of epoxy and lucite influence the transmission of radiation through the core; the amount of absorption is a function of spectral band width, numerical aperture and absorption coefficient. At an absorbing-nonabsorbing interface the influence of absorption upon Fresnel reflection is large at the critical angle and diminishes as the angle of incidence increases. Losses at any wavelength may be reduced if the magnitude of the absorption coefficient and the number of reflections or the length to diameter ratio is kept small. Such an approach allows ends of bundles to be potted and makes possible solid air tight fiber plates composed of fibers which can not be coated and therefore cannot be fused.

The ends of a light funnel of uncoated arsenic trisulfide fiber have been successfully potted in lucite. Also, silver chloride has been potted in lucite, however, tests have shown AgCl to be incompatible with some of the epoxies.

III. CONE CONDENSER

The theory of the cone condenser was presented in the first yearly report on this contract. Flux per unit area increases to be expected for a variety of cone designs and detector arrangements were presented in graphical form. Demonstration of the cone condenser efficiency in the infrared spectral region was undertaken as a phase of the present work. A germanium cone 25 mm in diameter at the base, 1 mm in diameter at the apex and 25 mm long was designed for the experiment because the higher refractive index has a larger potential flux gain than a silicon cone. An immersed PbS detector is required if the exceptionally large flux gains are to be observed; however, the conductivity of germanium is sufficient to short out an immersed PbS detector. To insulate the PbS from the germanium an intermediate coating of silicon was to be deposited on the germanium before the detector deposition. The PbS cells were to be deposited on the cone ends by Infrared Industries who expressed confidence in the success of the above deposition procedure. Concurrent with the fabrication of the above cone condensers, a cone transmitting to 2.8μ and designed to operate with an air spaced PbS detector was constructed. In addition, fabrication of a 3.1 inch long silicon cone having ends of 0.050inch and 0.745 inch diameter was completed. Deposition of a PbS detector on the smaller cone end and on two control silicon disks was to be made by Infrared Industries, Inc. The contract was terminated before any of the above experiments were completed.

IV. TRANSMISSION OF FIBER BUNDLES

A. Instrument Design.

The optical design of the instrument assemblied for measurement of the transmission of fiber bundles is shown in Figure 5. Radiation from a

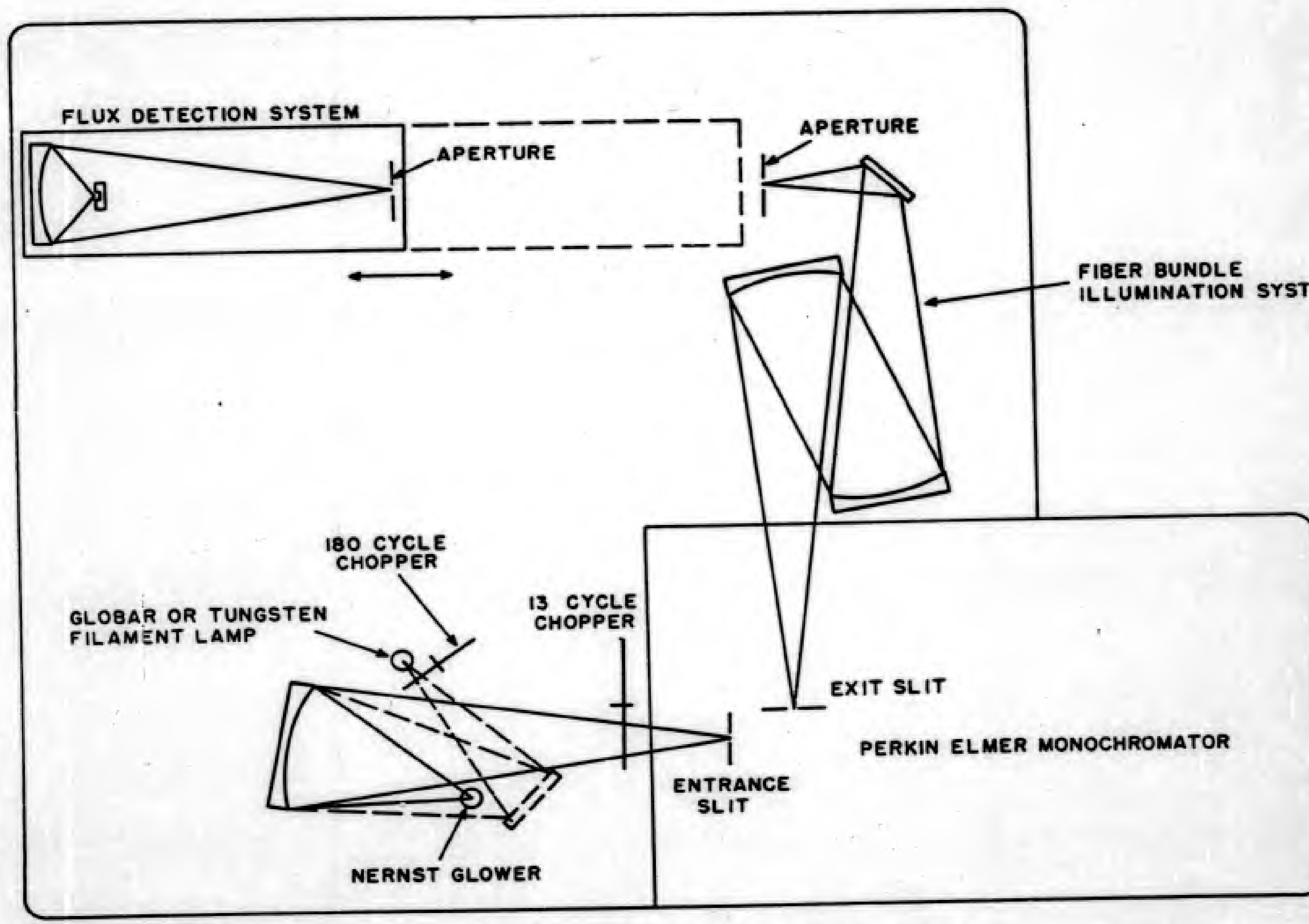

FIGURE 5. FIBER BUNDLE TRANSMISSION MEASUREMENT SYSTEM

Nernst Glower, a Globar or a tungsten filament lamp is imaged on the entrance slit of the Perkin-Elmer Monochromator. Radiation passing through the entrance slit is dispersed in the monochromator and then relayed by means of two spherical mirrors and a plane mirror to an aperture defining the sample area. Apertures corresponding to the geometry of the fiber optics device under test are interchangeable both in the fixed illumination system and the movable detection system.

A movable flux detection system employing an elliptical mirror images a second aperture onto a thermocouple detector as shown at the upper left of Figure 5. For the one hundred per cent reading, the detection aperture is brought into contact with the illumination defining aperture. The shape of the movable aperture must be equal to or larger than the aperture in the fixed optics and must accept radiation from all fibers which are initially illuminated. Fiber plates and bundles of fibers up to 10 inches long are accommodated by this instrument.

The movable flux detection system has functioned satisfactorily and the signal level using a LiF prism as the dispersive element in the monochromator is approximately 250 times the noise level when a 0.094 inch aperture is employed. Positioning of rods and bundles in between the apertures of the illumination and detection optics was found to be convenient. Reproducible transmission measurements have been made.

B. Transmission Measurements.

The spectral transmission of a fiber bundle composed of 0.003 inch diameter uncoated As_2S_3 fibers having ends potted in lucite is shown in Figure 6. Fiber packing at the bundle ends is good but the surface finish of the ends is not of optical quality because of the difference in hardness of the fiber and potting material. This bundle 68 mm long is compared to an As_2S_3 rod of 0.20 inch diameter and 32 mm length. Reflection losses at the entrance and exit ends are included in the transmission value which was measured for a convergent illumination cone of f/4.

The spectral transmission of a bundle of 0.005 inch diameter IR-20 fibers coated with optical glass is graphed in Figure 6. The transmission of this 79 mm long bundle is greater than 80 per cent between 1.6μ and 2.7μ. A fiber bundle of 65 mm length composed of uncoated fibers exhibited this same sharp cut off. In the uncoated fiber, this absorption cannot be attributed to the coating but must be due to the bulk absorption of the IR-20 glass. Transmission curves of bulk IR-20 indicate a value of about 60-79 per cent in the 3-5μ spectral region for a 4 mm thick sample, thus accounting for very low transmission in a 65 mm length.

V. ENERGY TRANSFER IN SMALL DIAMETER FIBER

A theoretical study of the mechanism of energy transfer in fibers has been continued. Theory predicts that, if two identical slabs are placed a short distance apart, energy transfer will occur. This prediction is confirmed experimentally in the frustrated total reflection filter where resonance

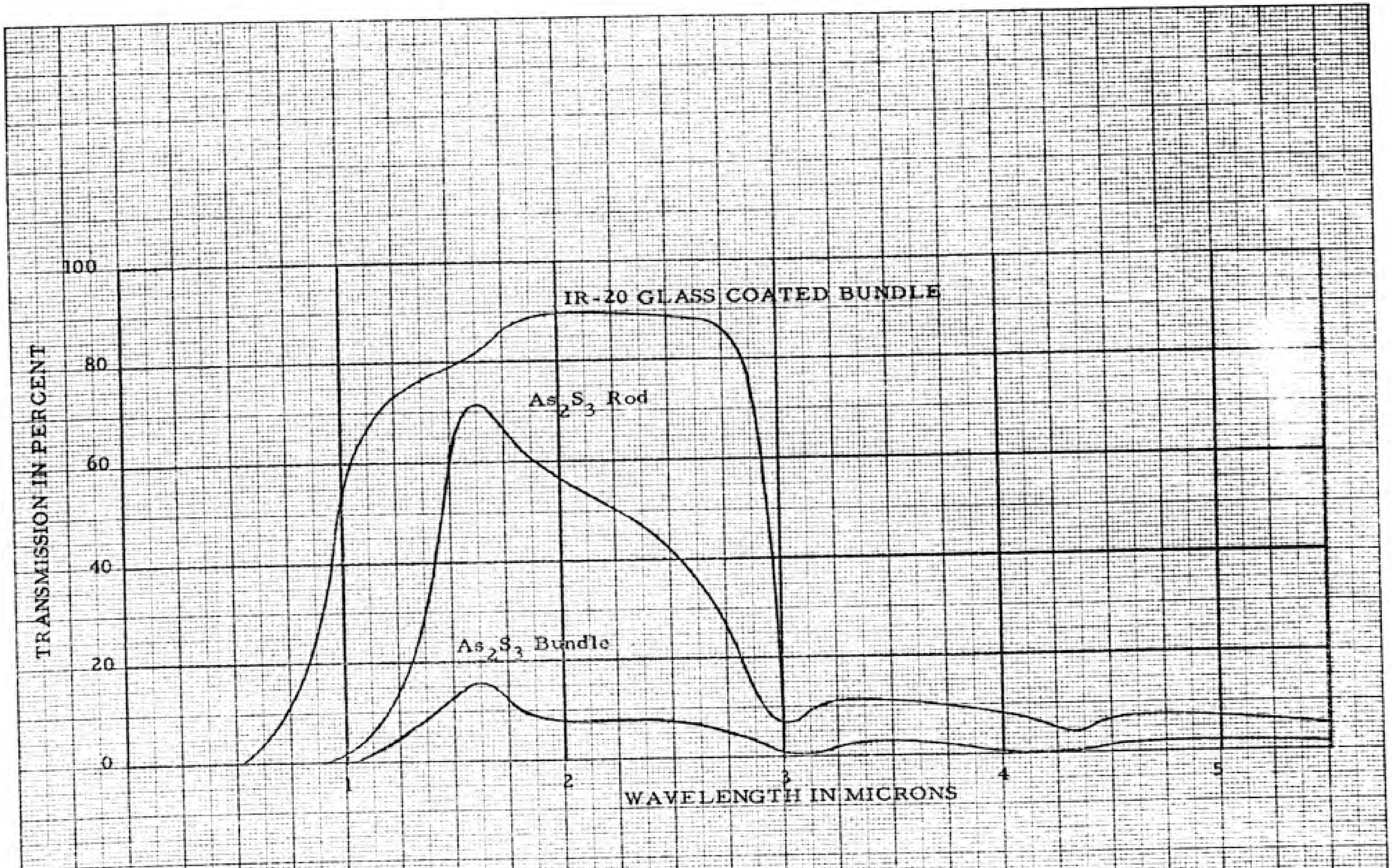

FIGURE 6. TRANSMISSION OF INFRARED FIBER OPTICS

transmission occurs whenever the ratio of the thickness to the wavelength satisfies certain conditions in spite of the reflecting layers. The bandwidths of these filters are very narrow, and the layers must be near perfect for this resonance transmission to occur.

In the same way, resonance transfer can occur in identical fibers. Because it has neither been necessary nor possible to maintain cross section and size constant over long fibers this resonance transfer had not been observed. Thus it appears that slight variation in fibers is to be desired, so as to frustrate resonance transfer.

Energy transmission of sub-wavelength fibers of approximately 2-5μ diameter can be investigated using radiation in the 1-10μ infrared spectral region. Experiment design requires the bulk capsulating material to transmit to longer wavelengths than the fiber material. However, in short lengths the fiber material must transmit in the extended spectral region of the outer material. Thus, for a short length following the fiber entrance end all wavelengths are transmitted by the fiber and wavelengths greater than or equal to the fiber diameter will be conducted in the capsulating material. The radiation is transmitted in the region exterior to the fiber and is attenuated less than it would have been if it had been transmitted by multiple total reflections within the fiber. Measurement of the radiation in narrow spectral bands transmitted by this type of assembly will test the theoretical predictions.

Combinations of materials suitable for this experiment are germanate (IR-20) or optical glass imbeded in Irtran AB-1 or Irtran ABC-II. The Irtran materials have the desired transmission and refractive index but are molded at temperatures in excess of the fiber melting point. Other optical potting materials having regions of absorption and transmission in the infrared spectral region have been found. For the most part, these compounds are plastics formed from solutions to which activators are added and which are then cured at relatively low temperatures. As they shrink upon curing, they are suitable for potting of fibers. Naturally, in their application to the sub-wavelength fiber problem, the measurement of externally transmitted radiation is made in regions where the plastic transmits.

The study of energy transfer between fibers in a close packed assembly continues to indicate that, in fibers of diameter greater than two wavelengths, it is possible to reduce leakage caused by frustrated total reflection to permit their effective use in a variety of applications.

In order that experiments performed on energy transfer between fibers yield completely unambiguous results, it is desirable that only one fiber in a given array be excited at any one time. This requires that the exciting energy be concentrated into a region no greater, in cross-section, than the fiber diameter. This, of course, is an impossible specification, for no conventional optical system can confine the energy emitted from a point source to anything less than the region specified by the Airy distribution, which is theoretically infinite, nor are any point sources available. In practice, one places the strongest available source behind a very small aperture, thereby approximating the ideal point source by a small relatively coherent disc source, and focuses this source on the entrance end of a single fiber. If the disc source is small enough (50 to 100 microns for microscope objectives of 50 to 100 power), the central portion of the Airy distribution will be concentrated within the radius of the single fiber while the remaining 16% of the available energy is diffracted onto the coating and the adjacent fibers. This is the optimal condition. Actual experimental arrangements force one to contend with some spherical aberration, with resultant diminution of the fraction of the total available energy which can be centered on a single fiber.

Since a very small hole is used as the disc source, the first limitation to total available flux is apparent. Much of this flux is reflected at the entrance plane of the fiber bundle, and a small portion of it is absorbed in passage down the fibers. In the earliest experiments, it was found that only the polychromatic mercury arc source was strong and stable enough to permit direct photoelectric measurement of the flux emanating from individual fibers, both those primarily excited and those adjacent to them. These measurements were made on linear arrays of small fibers, and on hexogonal arrays. Relative flux between excited and adjacent fiber did not exceed 13:1. This figure, however, has questionable meaning without the application of some corrections to account for: 1) the fraction of the flux emanating from a secondarily excited fiber which results from excitation by the source (Airy disc) at its entrance end, as opposed to leakage from the excited fiber; 2) spectral response of the photomultiplier; 3) spectral response of the fiber bundle itself, both in relative absorption and relative leakage. In order to correct for the first term, it is necessary to measure the point spread function of the exciting microscope. Such measurements, being wavelength dependent, prove inconclusive. It was, therefore, decided to attempt to improve on the conventional optics of the measuring system and the sensitivity of the electronics to a sufficient degree to permit the use of the strongest available monochromatic source, a sodium arc lamp.

In the above experiments, the excitation of a single fiber is accomplished by microscopic imaging of a pin hole on its entrance end. Because of diffraction and scattering in the microscope objective, however, some excitation of adjacent fibers is unavoidable. Therefore, an attempt was made to deposit a sub-micron pin hole in a layer of aluminum at the entrance end of the fiber. This is achieved by placing a number of submicron polystyrene spheres on top of the fiber assembly and depositing aluminum on it in a high vacuum evaporating unit. The polystyrene spheres are then blown away, thus leaving pin holes as small as 0.1μ in diameter. Although a number of pin holes were thus placed on different diameter fibers and the fiber coupling was observed by illuminating these pin holes, the results are considered inconclusive. This was primarily because the positioning of the submicron pin holes with respect to the fibers could not be determined exactly. In addition, the diffraction arising at the submicron metallic pin hole at the entrance end of the fiber yields drastically different excitation conditions than would be encountered by fibers during their normal use in optical systems. Furthermore, the light levels under these conditions were so low as to render photoelectric photometry of flux in adjacent fibers very difficult.

In view of these problems, it was decided that only one reliable data run could be obtained. These data would be the result of measurements which compared the total flux emanating from the excited fiber with the total flux from that fiber and the six surrounding fibers. To this end, assemblies of circular fibers in almost perfect hexagonal array were fabricated. With the apparatus shown in Figure 7, an Airy disc-like image of a 100 micron pin hole, illuminated by a Sodium arc source, was centered on one fiber. The image of the exit ends of this excited fiber and the adjacent ones was focused in the plane of an iris diaphragm, which was directly in front of the photo-cathode of a photomultiplier. (The variable slit in Figure 7 was replaced by this diaphragm.) The opening of the diaphragm was first set to include only the image of the excited fiber, and a reading of the flux from this fiber was taken. The diaphragm was then opened to include the six adjacent fibers, and a second reading was made. One-sixth of the difference between these two flux measurements represents the average emanating from adjacent fiber. The ratio of this to the flux from the excited fiber would give the average leakage from the excited to an adjacent fiber, were it not for the direct excitation of the adjacent fiber caused by diffraction and scattering in the exciting microscope. To obtain a measure of this, the fiber bundle was removed and the detecting system was moved forward a distance equal to the fiber length (about one inch). The image of the excitation condition was thus formed at the photocathode with the same magnification as the image of the

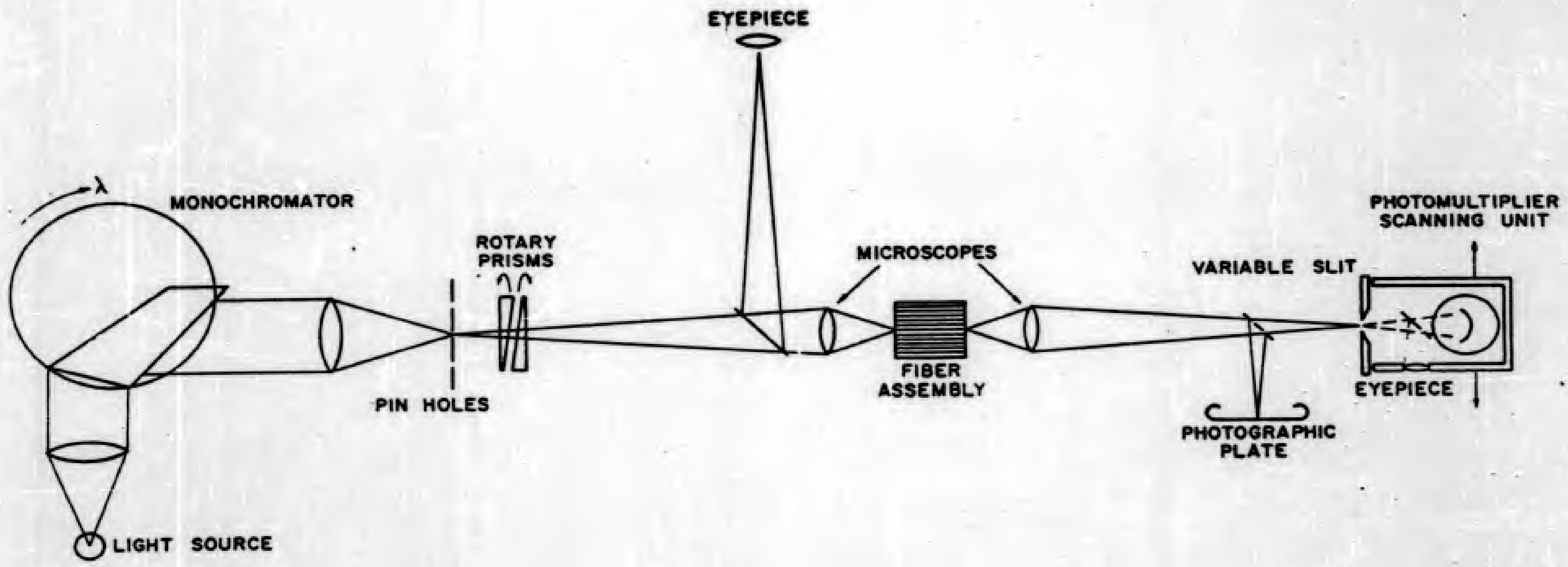

FIGURE 7. APPARATUS FOR STUDYING SMALL DIAMETER FIBER SYSTEMS.

previously measured bundle. Two measurements of the flux with the same iris diaphragm settings as those used on the fiber bundle were then made. From the difference of these, a rough measure of the relative primary excitation of the central and the adjacent fibers was obtainable. The following table gives the results of these experiments. The quantity A gives the average ratio of the flux (in per cent) from an adjacent fiber to that in the centrally excited fiber. The measurements on a given fiber were repeatable to within 4 to 5 per cent. Measurements of different fibers in the bundle differed by as much as a factor or two. There was no correlation between these rather large differences in A and the slight variation of fiber diameters and spacings in the bundle. The differences are thus assumed to be caused by variations in surface quality from fiber to fiber. The quantity A' is a measure of the relative primary excitation of the adjacent and central fibers. R is the "fiber characteristic term" = $\frac{d}{\lambda}\left(N_1^2 - N_2^2\right)^{1/2}$.

n_1	n_2	diameter	spacing	A(%)	A'(%)	R
1.9	1.53	1.98	0.4	$3.6 \pm .7$	2.4	15
1.9	1.53	3.84	1.07	0.25	1	28
1.564	1.484	3.5	0.45	$4.1 \pm .9$	1	8.5

From this table it is clear that the coupling between fibers is a very strong function of the term R and the fiber separation. When the value of R is high, the coupling is low and, therefore, the fiber assembly is capable of higher image quality. One micron diameter fibers of $N_1 = 1.90$ and $N_2 = 1.50$ with a fiber separation of less than 1μ have shown only small amounts of coupling and an assembly of them has yielded 400 lines/mm static and 800 lines/mm dynamic resolution under white light conditions.

The performance of fibers of diameter comparable to the wavelength has been analyzed by using dielectric waveguide theory and the results have been interpreted from the optical viewpoint of thin film interference and frustrated total reflection. The theoretical results of these studies are presented in Appendix A along with additional experimental data.

VI. CONCLUSION

Vitreous infrared transmitting materials have been drawn into coated and uncoated fibers by employing techniques developed for the formation of visible radiation transmitting glass coated-glass fiber. Numerous materials transmit in the infrared spectral region, however, only a few vitreous materials are suitable for drawing fiber from rod and tube configurations in a vertical furnace. Materials which have been drawn into uncoated fiber of 25-100μ diameter are arsenic trisulfide, IR-20 and IR-2. Fiber composed of IR-20 cores coated with optical crown glass or IR-2 have been drawn in extended lengths. Also, short fiber lengths of arsenic trisulfide cores coated with an arsenic sulfide material have been successfully drawn.

Of the crystalline materials, silver chloride has been extruded into 0.010 inch diameters in short lengths. However, the surface finish is not of optical quality. Magnesium oxide formed into rectangular rods suggests another way in which crystalline materials may be employed in fiber optics. Here, mass production of the rods could reduce the cost of individual elements sufficiently to permit the fabrication of fiber optics face plates. These plates would require the rods of the crystalline material to be potted in a matrix material of hardness similar to that of the rod since this is a requirement for grinding and polishing of the plates.

Plastic materials such as the epoxies and lucite are suitable materials for potting uncoated fiber. The absorption bands do not seriously influence the transmission of radiation in short fiber lengths, however, in longer fiber the effects of absorption bands can be expected to be pronounced. When broad wavelength band transmission is desired the potting materials must have few absorption bands in the region of interest. In all cases, the potting compounds must be non-scattering and must wet the fiber surface. A number of fiber bundles were prepared in which only the ends of the bundles were potted. In these cases there was not an observable absorption which could be attributed to the matrix material.

The optical performance of small-diameter fibers has been successfully analyzed by an extension of existing waveguide theory. The problem has been treated from the conventional optical viewpoint of interference and frustrated total reflection. It is shown that the "characteristic waves" or modes are made up of elementary plane waves which are propagated at discrete angles down the fiber and that these angles are determined by the characteristic equations of the waveguides. The number of allowed characteristic angles and the optical diameter are dependent on the "fiber-characteristic term" which is the product of the fiber numerical aperture, the diameter-to-wavelength ratio and π. The value of this product, for a given mode, is directly proportional to the permissible angles and inversely proportional to the optical diameter. The lower limit to the fiber diameter (circular cross-section fibers are preferable to other configurations) for an image-conveying system is determined by the "fiber characteristic term" and the fiber spacing. The experimental results indicate that fibers of high numerical aperture down to 1μ in diameter can yield high image quality. Such fiber bundles have yielded resolutions of 400-800 lines per mm. Long isolated fibers down to 0.1μ diameter have conducted light, however, they are not efficient for image transmission because their optical diameter is large. With the availability of higher numerical aperture fibers of circular cross section and development of techniques for fabricating aligned assemblies of them, it seems possible to achieve substantially higher resolution in fiber optics for all spectral regions.

VII. LOGBOOKS AND CONTRIBUTING PERSONNEL

Work on this contract is recorded in Armour Research Foundation Logbooks C-9319, C-9726, C-9891, C-9965, C-9970, and C-10224.

Staff members of Armour Research Foundation who contributed to the work reported during this period include: A. Brushenko, J. Burke, N. S. Kapany, A. Leeds, F. X. Miller, K. O'Brien, and D. A. Pontarelli.

Respectfully submitted:

ARMOUR RESEARCH FOUNDATION
of Illinois Institute of Technology

D A Pontarelli

D. A. Pontarelli, Research Physicist
Optics Research

P H Wyckoff

P. H. Wyckoff, Acting Supervisor
Optics Research

APPROVED BY:

P H Wyckoff

P. H. Wyckoff
Assistant Director of Physics Research

APPENDIX A

WAVEGUIDE EFFECTS

JOURNAL OF THE OPTICAL SOCIETY OF AMERICA VOLUME 51, NUMBER 10 OCTOBER, 1961

Fiber Optics. IX. Waveguide Effects*†

N. S. KAPANY‡ AND J. J. BURKE‡
Physics Division, Armour Research Foundation, Chicago, Illinois
(Received November 29, 1960)

In recent years techniques for fabricating fibers of diameter comparable to the wavelength have been developed in order to achieve high-resolution fiber optical systems. The performance of such fibers is analyzed by using dielectric waveguide theory, and the results are interpreted from the optical viewpoint of thin film interference and frustrated total reflection. The energy distributions inside (mode pattern) and outside such fibers are computed as a function of the fiber parameters, and the interaction of energy between neighboring fibers is considered. Experimental measurements of the fiber spread function are made for assemblies of close-packed fibers, and its dependence on fiber diameter (d), spacing (t), wavelength (λ), and indices of refraction (n_1 and n_2) is investigated. It is shown that the "optical diameter" of fibers and the number of modes propagated is critically dependent on the "fiber characteristic term" R given by

$$R=(\pi d/\lambda)(n_1^2-n_2^2)^{\frac{1}{2}}.$$

I. INTRODUCTION

In the early stages of development of fiber optics, when the diameters of the fibers being fabricated were many times the wavelengths of light, the optical performance of fibers was described in terms of geometrical optics.[1,2] In this treatment it is assumed that rays traveling down a fiber of index n_1 coated with a layer of glass of index $n_2<n_1$ are totally internally reflected at the core-coating interface if their angles of incidence at this interface are greater than the critical angle, $\theta_c=\sin^{-1}n_2/n_1$, and that the energy associated with these rays is conducted down the length of the fiber. To account for energy losses caused by imperfections in the core-coating interface and absorption in the fiber material, appropriate scattering and absorption terms are applied. In addition, the physical optics effects of field penetration into the coating (the evanescent wave) and the resultant leakage of energy to neighboring close-packed fibers are incorporated into the theory through the inclusion of terms specifying the extent of the frustrated total reflection losses.[3] These terms are based on the Fresnel transmission formula for the case of plane waves incident upon a totally reflecting layer separating two plane-parallel high-refractive-index media. They are thus accurate to the extent that the core-coating interface can be approximated by a plane. To find the transmittance of the fiber, the effects of all incident rays are integrated.

With advent of techniques for fabrication of micron- and submicron-diameter fibers,[4] a return to the more fundamental approach of Maxwell's theory became necessary. It resulted in the reinvestigation of the theory of the circular cylinder dielectric waveguide, first formulated by Carson *et al.*[5] in connection with microwave studies. Numerous experimental and theoretical investigations of the waveguide modes of these cylinders have since been reported. It is our purpose at this time to extend further the dielectric-waveguide analysis as applied to circular fibers, and to reinterpret the "mode" descriptions of fiber performance from the more familiar optical viewpoints of frustrated total reflection and interference. Optical interpretation of waveguide theory has been made in part by others in the past, in particular by Page and Adams[6]. What will be presented here, then, is an extension of both the analysis and the optical interpretation of waveguide effects in fiber optics. It will be seen that this optical interpretation of waveguide theory permits the understanding of fiber performance in precisely the same terms as in the earlier theory,[3] and that from it rough predictions can be made of the energy-transfer properties of arrays of fibers.

The second part of this paper will review the waveguide solutions for the permissible propagating waves of the dielectric cylinder, and will point out the nature and form of these waves in optical terms. The third part will be devoted to extending the results of waveguide theory as applied to fiber optics. Finally, the results of experiments in support of the theory will be given and measurements of fiber spread function due to the coupling phenomenon will be presented. Various factors affecting the lower limit to the fiber diameter set by the coupling process are discussed.

II. NATURE OF THE WAVEGUIDE SOLUTION

The waveguide theory answers questions regarding the natural modes in which energy is propagated down a glass-coated glass fiber. Problems involving how the energy enters or emerges from a fiber of finite length are not considered in the initial formulation. This is accomplished by assuming an isolated circular cylinder

* This work was presented in two papers at the Forty-Fifth Annual Meeting of the Optical Society of America, Boston, Massachusetts, October 12, 1960.

† This work has been sponsored by an Air Force contract, Wright Air Development Division, Dayton, Ohio.

‡ Now at Optics Technology, Inc., 248 Harbor Boulevard, Belmont, California.

[1] N. S. Kapany, in *Concepts of Classical Optics*, edited by J. Strong (W. H. Freeman and Company, San Francisco, California, 1958).
[2] N. S. Kapany, J. Opt. Soc. Am. 47, 5, 413 (1957).
[3] N. S. Kapany, J. Opt. Soc. Am. 49, 8, 770 (1959).
[4] N. S. Kapany, Nature 184, 881 (1959).
[5] J. R. Carson, S. P. Mead, and S. A. Schelkunoff, Bell System Tech. J. 15, 310 (1936).
[6] L. Page, and N. I. Adams, Jr., Phys. Rev. 52, 647 (1937).

of infinite length with index of refraction n_1 embedded in an infinite medium of index $n_2<n_1$.

It is assumed that any disturbance propagated down the fiber must satisfy Maxwell's equations inside and outside the fiber core, and that the tangential components of **E** and **H** must be continuous across the interface separating the core and the coating. In order that this isolated fiber trap the energy, it is also required that the time average radiation across the fiber wall be zero. For convenience, it is also assumed that the materials of core and coating have zero conductivity and equal magnetic permeability. With these assumptions in view, the homogeneous wave equations for the core and coating are solved in a straightforward manner.[7] They are readily separable when written in terms of cylindrical coordinates (r,φ,z), where the z axis is assumed to be coincident with the fiber axis. The separation constants for the t, z, and φ dependences are $-\omega^2$, $-h^2$, and $-n^2$, respectively. The angular frequency ω may assume any value. The parameter n must be a positive or negative integer or zero. The propagation constant in the axial direction, h, is restricted to take on only certain discrete values h_{np}. Corresponding to each such eigenvalue there are two eigenfunctions, one with even azimuth dependence (i.e., $\cos n\varphi$) and one with odd azimuth dependence ($\sin n\varphi$). The general solution to the problem may be expressed as a sum over these eigenfunctions. The sum is finite, since there is a maximum value of n corresponding to the greatest value of n for which the characteristic equation (to be discussed later) yields a root. For each n there is a maximum value of p. The sum over p is thus also finite. The total number of eigenfunctions depends on the fiber diameter, the wavelength, and the indices of refraction of core and coating. A single eigenfunction is labeled by the subscripts np and the superscript e (even) or o (odd). Any one of the six field components may be considered as a single eigenfunction, since once it is specified, all the others are fixed. We choose the z component of E as the eigenfunction, and relate the others to it. This eigenfunction takes one form for the fiber core and another for the coating, as do all the field components. In the fiber core, the field components corresponding to the even (cos) and odd (sin) eigenfunctions with eigenvalue h_{np} are given by Eqs. (1), in which the commas should be read as "or."

$$
\left.
\begin{aligned}
{}_zE_{np}{}^{e,o}&=(+B_{np}{}^{e}\cos,\ +B_{np}{}^{o}\sin)F_{np}[J_n]\\
{}_zH_{np}{}^{e,o}&=(-B_{np}{}^{e}\sin,\ +B_{np}{}^{o}\cos)F_{np}[J_n][h_{np}A_{np}/\omega\mu]\\
{}_rH_{np}{}^{e,o}&=(-B_{np}{}^{e}\sin,\ +B_{np}{}^{o}\cos)F_{np}[(k_1{}^2-h_{np}{}^2A_{np})J_{n-1}+(k_1{}^2+h_{np}{}^2A_{np})J_{n+1}][i/2\omega\mu\beta_{np}]\\
{}_\varphi H_{np}{}^{e,o}&=(+B_{np}{}^{e}\cos,\ +B_{np}{}^{o}\sin)F_{np}[(k_1{}^2-h_{np}{}^2A_{np})J_{n-1}-(k_1{}^2+h_{np}{}^2A_{np})J_{n+1}][-i/2\omega\mu\beta_{np}]\\
{}_rE_{np}{}^{e,o}&=(+B_{np}{}^{e}\cos,\ +B_{np}{}^{o}\sin)F_{np}[(1-A_{np})J_{n-1}-(1+A_{np})J_{n+1}][-ih_{np}/2\beta_{np}]\\
{}_\varphi E_{np}{}^{e,o}&=(+B_{np}{}^{e}\sin,\ -B_{np}{}^{o}\cos)F_{np}[(1-A_{np})J_{n-1}+(1+A_{np})J_{n+1}][ih_{np}/2\beta_{np}].
\end{aligned}
\right\}
\quad (1)
$$

Here

$$F_{np}=\exp(i\omega t-ih_{np}z);\quad \beta_{np}{}^2+h_{np}{}^2=k_1{}^2=\omega^2\epsilon_1\mu$$

$$\text{Argument of } J_{n,n-1,n+1}=\beta_{np}r;\quad \text{argument of } \sin,\cos=n\varphi.,$$

The fields outside the fiber core have a similar form. If the equation $r=a=d/2$ defines the core-coating interface, then the fields for $r>a$ may be obtained from Eqs. (1) by the following substitutions:

$$B_{np}{}^{e,o}\rightarrow B_{np}{}^{e,o}\frac{J_n(\beta_{np}a)}{K_n(\beta_{np}'a)};\quad \beta_{np}\rightarrow\beta_{np}';\quad k_1\rightarrow k_2;$$

$$J_n\rightarrow K_n;\quad J_{n\pm1}\rightarrow\mp K_{n\pm1},$$

where

$$h_{np}{}^2-\beta_{np}{}'^2=k_2{}^2=\omega^2\epsilon_2\mu.$$

Equations (1) express the field components in such a manner that the first factor gives the azimuth (φ) dependence, the second the axial (z) and time (t) dependences, the third the radial (r) dependence, and the last the appropriate proportionality factors. In the azimuth factor, the B's are constant amplitude factors determined by the excitation condition. The azimuthal dependence of an eigenfunction may thus have the form $B_{np}{}^{e}\cos(n\varphi)$ or $B_{np}{}^{o}\sin(n\varphi)$ or any combinations of these. The second factor indicates that the fields are those of traveling waves whose planes of constant phase are perpendicular to the fiber axis and propagate with a velocity ω/h_{np} in the direction of positive z. In the radial factors, the J's are Bessel functions of the first kind, with the subscripts indicating their order. The K's are modified Bessel functions of the second kind which, for large argument, have the approximate form $(1/\beta_{np}'r)^{\frac{1}{2}}\exp(-\beta_{np}'r)$. These functions are proportional to the Hankel function of imaginary argument. The constant A_{np} is fixed by the eigenvalue h_{np}. An expression from which its value may be determined is given with Eq. (11), in that section of the paper where the intensity distribution in the fiber cross section is discussed. It may be seen that when its value may be approximated by ±1, the fields in the fiber cross section take on a particularly simple form, being proportional to either J_{n-1} or J_{n+1}. In such cases the intensity distribution in any plane perpendic-

[7] J. A. Stratton, *Electromagnetic Theory* (McGraw-Hill Book Company, Inc., New York, 1941).

ular to the fiber axis is circularly symmetric, and the polarization of the E vector in the fiber cross section is considerably simplified. Thus,

$$\left.\begin{aligned} &\text{if } A_{np}=1, \text{ then } {}_xE_{np}^e\to\cos[(n+1)\varphi]J_{n+1} \\ &\qquad\text{and } {}_yE_{np}^e\to\sin[(n+1)\varphi]J_{n+1} \\ &\text{if } A_{np}=-1, \text{ then } {}_xE_{np}^e\to -\cos[(n-1)\varphi]J_{n-1} \\ &\qquad\text{and } {}_yE_{np}^e\to\sin[(n-1)\varphi]J_{n-1} \end{aligned}\right\}. \quad (2)$$

Either of conditions (2) may be rigorously satisfied in the limit as the ratio of the indices of core and coating approaches unity. That is, there exists in the limit a set of eigenvalues and corresponding eigenfunctions with constant $A_{np}=1$, and a second set of eigenvalues and corresponding eigenfunctions with constant $A_{np}=-1$. According to this limiting behavior of A_{np}, the eigenfunctions are usually classified as either EH_{nm} modes with eigenvalues h_{nm}^+ or as HE_{nm} modes with eigenvalues h_{nm}^-, $m=1, 2, 3, \cdots$. In terms of Eqs. (1), $h_{n1}^-=h_{n1}$; $h_{n1}^+=h_{n2}$; $h_{n2}^-=h_{n3}$, etc., the + and − eigenvalues alternating.

Generally the modes of the dielectric cylinder are hybrid, that is, both E and H have longitudinal components. However, when the fields do not depend on azimuth, i.e., when $n=0$, a pure E wave ($H_z=0$) or a pure H wave ($E_z=0$) may exist. The H wave may be obtained from Eqs. (1) by letting all the amplitude factors $B_{op}^{e,o}$ go to zero while the A_{op} factors go to infinity in such a way that the product $B_{op}A_{op}$ may take on any arbitrary constant value. The E wave is given by Eqs. (1) with $A_{op}=0$ and the B_{op} arbitrary constants. It is seen that for the case $n=0$ the even-odd degeneracy of the eigenfunctions is removed, there being only one eigenfunction for each eigenvalue h_{op}. Again, in the notation generally in use, these are referred to as H_{om} (also TE_{om}) modes or E_{om} (also TM_{om}) modes.

The nature of the solution will now be indicated. It will be shown that these waveguide modes are made up of elementary uniform plane waves whose wave normals (rays) make certain characteristic angles with the normal to the fiber wall and that these angles are to be found from the roots of the characteristic equation mentioned above. For convenience in illustrating this, it will be assumed that a condition has been achieved experimentally in which only one mode is present in the fiber. This mode, the H_{om} mode, is described by Eqs. (3) in which the constants of Eqs. (1) are contracted into the simple form A_{om}', C_{om}'.

$$\left.\begin{aligned} &\text{Core}\begin{cases} H_z=A_{om}'J_0(\beta_{om}r)\exp(-i\omega t+ih_{om}z) \\ E_z=0 \end{cases} \\ &\text{Coating}\begin{cases} H_z=C_{om}'K_0(\beta_{om}'r)\exp(-i\omega t+ih_{om}z) \\ E_z=0 \end{cases} \end{aligned}\right\} \quad (3)$$

$$\beta_{om}=k_1\cos\theta_{om};\quad h_{om}=k_1\sin\theta_{om}. \quad (4)$$

If we define the angle θ_{om} by Eq. (4) we may decompose this wave into its component parts with the use of an integral form of the function J_0. This is done in Eqs. (5).

$$\left.\begin{aligned} H_z&=\frac{\exp(-i\omega t)}{2\pi}\int_0^{2\pi}A_{om}'\exp(irk_1\cos\theta_{om}\cos(s-\epsilon)+izk_1\sin\theta_{om})ds \\ H_z&=\frac{\exp(-i\omega t)}{2\pi}\int_0^{2\pi}A_{om}'\exp(i\mathbf{k}_{1om}(s)\cdot\mathbf{r})ds \\ \mathbf{k}_{1om}(s)&=[k_1\sin(\pi/2-\theta_{om})\cos s,\ k_1\sin(\pi/2-\theta_{om})\sin s,\ k_1\cos(\pi/2-\theta_{om})] \end{aligned}\right\}. \quad (5)$$

These equations show that the H_{om} mode is made up of certain uniform plane waves, all of the same amplitude, A_{om}', but with wave normals $\mathbf{k}_{1om}(s)$ in different directions. It may be seen that all these wave normals make the same angle $(\pi/2-\theta_{om})$ with the fiber axis, and that only their azimuth directions s vary. If we adopt the custom of calling these wave normals rays, we see that a given ray traveling in azimuth direction s makes an angle θ_{om} with the normal to the fiber wall, and may be associated with a plane wave incident upon that wall. Another ray with opposite azimuth, $\pi+s$, also included in the integration, may be associated with the reflected wave corresponding to this incident wave. The integral over all azimuths of these uniform plane waves is thus seen to be merely a representation of all the E_1 meridional rays which strike the wall at angle θ_{om}. The interference of these uniform plane waves will result in an interference pattern in the fiber cross section in the form of circular rings. Such an interference pattern is the fiber mode pattern of the H_{om} wave. (The appendix to this paper contains another approach to the incident and reflected wave interpretation of waveguide modes. This second approach may provide a clearer insight into their nature.)

The general equations (6) indicate the plane waves which make up a given HE_{nm}^e hybrid mode. The first set are the plane waves which provide the z component of $\mathbf{H}$. The second set contribute the z component of $\mathbf{E}$. Both sets must be present to satisfy the boundary conditions.

$$\left.\begin{aligned} A_{nm}'J_n(\beta_{nm}r)\sin n\varphi\exp(-i\omega t+ih_{nm}z)&=\frac{i^{-n}\exp(-i\omega t)}{2\pi}\int_0^{2\pi}A_{nm}'\sin ns\exp[ik_{nm}(s)\cdot\mathbf{r}]ds\\ B_{nm}^eJ_n(\beta_{nm}r)\cos n\varphi\exp(-i\omega t+ih_{nm}z)&=\frac{i^{-n}\exp(-i\omega t)}{2\pi}\int_0^{2\pi}B_{nm}^e\cos ns\exp[ik_{nm}(s)\cdot\mathbf{r}]ds \end{aligned}\right\}. \tag{6}$$

Note that the associated rays are all meridional and that all of them make the same angle θ_{nm} with the normal to the fiber wall, but that their amplitude varies sinusoidally with azimuth. The interference pattern arising from the addition of all these plane waves will thus also vary with azimuth. (For a complete discussion of the plane wave decomposition of the cylindrical functions, the reader is referred to reference 7.)

The penetration of energy into the coating is described by the function K_n. This function serves the very same purpose in cylindrical geometry that the negative exponential serves in Cartesian geometry. (See Appendix.) It provides an approximately exponential decay in the amplitude of the fields outside the fiber core. The analogs in plane and cylindrical geometry are shown in Fig. 1. Figure 1(a) shows a plane wave incident upon a plane interface at an angle θ, and the corresponding reflected and evanescent waves. The wave fronts (planes of constant phase) are represented by dotted lines. The arrows designate the wave normals, their length indicating the amplitude of the time-average Poynting vector (the flux of energy per unit area), and their direction the direction of energy flow. In the incident medium, the superposition of incident and reflected waves gives a resultant wave whose planes of constant phase are perpendicular to the interface, and whose Poynting vector is parallel to the boundary and has a sinusoidally varying amplitude. In the second medium, the wave front is also perpendicular to the boundary, but with an intensity which decreases exponentially with distance from the interface. Thus, although some energy is carried along the interface outside the incident medium, most of it is very close to the interface. Figure 1(b) shows the analogous phenomena in fibers.

The differences between the geometrical and the waveguide theory are now apparent. There are, in fact, only two main differences. (1) The geometrical theory neglects phase information and thus cannot predict interference phenomena. (2) Whereas the more rigorous waveguide theory requires that one form the general solution by summing over certain discrete meridional rays, the geometrical approach assumes that all rays in the range of angles from $\pi/2$ to critical angle are possible. For fibers more than a few times the wavelength of light, the difference between predictions made from the two approaches will not be great under most optical excitation conditions. For small fibers, however, where only a few permissible characteristic angles exist, and an appreciable degree of coherence is attainable, the differences become apparent.

III. EXTENSION OF RESULTS OF THE THEORY

A. The Characteristic Equation and the "Fiber Characteristic Term"

In order to determine the characteristic angles for the permissible "rays" of a given fiber, transcendental Eq. (7) must be solved.

$$\frac{J_{n-1}(u)}{J_n(u)}=\frac{n}{u}+\left(1-\frac{\delta}{2}\right)\left(\frac{u}{q}\frac{K_{n-1}(q)}{K_n(q)}+\frac{nu}{q^2}\right)\pm\left[\frac{n^2R^2}{q^4}\left(\frac{R^2}{u^2}-\delta\right)+\frac{\delta^2}{4}\left(\frac{u}{q}\frac{K_{n-1}(q)}{K_n(q)}+\frac{nu}{q^2}\right)^2\right]^{\frac{1}{2}} \tag{7}$$

$$\left.\begin{aligned} R&=\frac{\pi d}{\lambda_0}(n_1^2-n_2^2)^{\frac{1}{2}};\quad \delta=1-\frac{n_2^2}{n_1^2}\\ u&=\frac{\beta d}{2};\quad q=\frac{\beta' d}{2};\quad q^2=R^2-u^2 \end{aligned}\right\} \tag{8}$$

$$\theta=\cos^{-1}\left[\frac{u}{(\pi d/\lambda_0)n}\right]. \tag{9}$$

If each side is plotted as a function of u, the intersections of the curves representing the two sides give those values of u which satisfy the equation and therefore the boundary conditions of the problem. Figure 2 illustrates the graphical solution for particular cases with n equal to 0, [Fig. 2(a)] and n equal to 1, 3, 5, 7, [Fig. 2(b)]. In the latter case only the first branch of J_{n-1}/J_n is shown.

The form of the characteristic equation given here is considerably different from that given in the literature.[7]

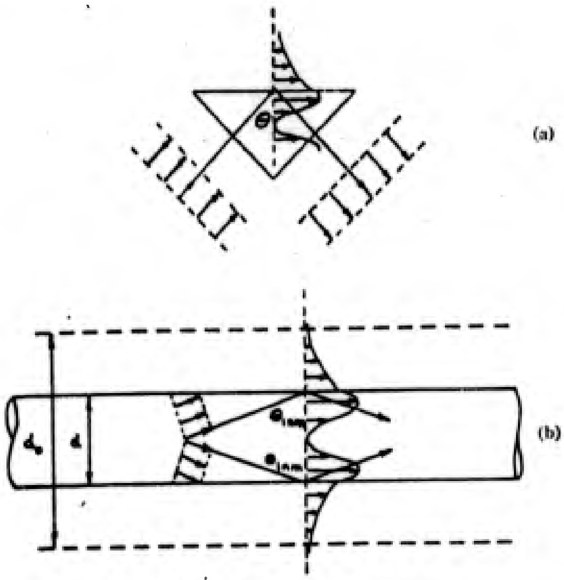

FIG. 1. Illustration of analogous interference and evanescent wave phenomena at (a) plane interface and (b) cylindrical fiber boundary.

This one is obtained from the more familiar form by the technique of completing the square. The form given here has the advantage of indicating at once that the characteristic equation is in fact two equations and thus provides two independent sets of solutions. Thus, for a given integer n, the mth root u_{nm}^{+} of Eq. (7) with the positive sign taken on the radical, yields the characteristic angle θ_{nm}^{+} of the EH_{nm} mode [by Eq. (9)], while the mth root u_{nm}^{-} of Eq. (7) with the negative sign taken on the radical yields the characteristic angle θ_{nm}^{-} of the HE_{nm} mode.

The terms in Eq. (7) are explained in Eq. (8). The parameters R and δ are determined by the fiber diameter, refractive indices, and wavelength under consideration. "q" is seen to be a function of u and R. The parameter R, termed the "fiber characteristic term," is of primary importance in the analysis of fibers of small diameter. This may be seen from the following argument:

For $u>R$, characteristic Eq. (7) has no solutions. As u approaches R, the right-hand side of Eq. (7) with the positive sign taken on the radical approaches infinity. Thus the maximum value of n for an EH_{nm} mode is that greatest integer N for which the equation $J_N(u)$ has one and only one root in the range $0<u<R$. (Although $u=0$ satisfies the characteristic equation, the condition that the fields vanish at $r=$ infinity causes them to vanish everywhere for this root.) For this value (N) of n, the maximum value of m is thus 1. For EH_{nm} modes with $n<N$, the maximum value of m equals the number of roots of the equation $J_n(u)=0$ which lie in the range $0<u<R$. For R less than the first nonzero root of J_1 (i.e., 3.832), there are no EH modes. For R less than the first root of J_0 (i.e., 2.405), no E_{om} or H_{om} modes are defined.

The number of HE waves is more difficult to specify. The HE_{11} mode may exist in any fiber, no matter how small, though as d/λ_0 decreases below 1/2, θ_{11}^{-} rapidly approaches the critical angle and most of the energy is outside the fiber core. Generally, if the EH_{nm} mode is defined, the HE_{nm} mode also exists. The simplest means of determining whether or not the $HE_{n(m+1)}$ mode exists is to do so visually by examining the separation between levels on a chart of eigenvalues. Such charts are given in Fig. 3 and will be discussed shortly. It should be noted that, unlike the eigenfunctions of the metallic tube, the eigenfunctions of the dielectric cylinder do not form a complete set and cannot, therefore, describe the most general disturbance in the fiber and its surround.

R is seen to be a function of the diameter-to-wavelength ratio and the fiber numerical aperture, N.A. $=(n_1^2-n_2^2)^{\frac{1}{2}}$. As it decreases, the number of propagating

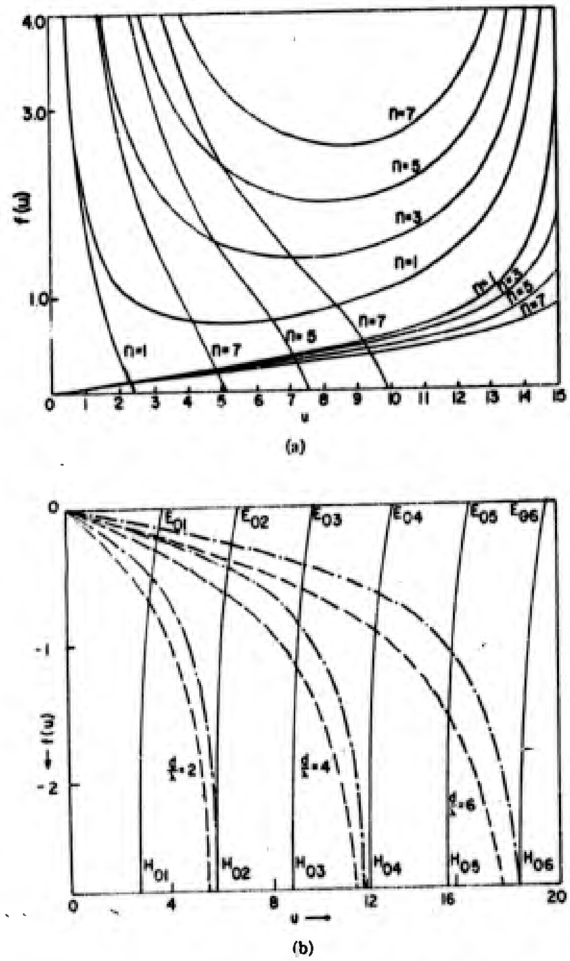

FIG. 2. Graphical solution of the characteristic equation (7). (a) $n=0$; $d/\lambda=2$, 4, 6; $n_1=1.8$, $n_2=1.5$. Solid curves represent the left-hand side of Eq. (7). Dashed curves represent the right-hand side with the negative sign taken on the radical; curves of alternating dots and dashes represent the right-hand side with the positive sign on the radical. (b) $n=1$, 3, 5, 7; $d/\lambda=4$; $n_1=1.9$, $n_2=1.46$. Lower four curves represent the right-hand side of Eq. (7) with the negative sign on the radical; upper curves take the positive sign. The first branch of the left-hand side of Eq. (7) for the four n values is shown by the curves which cut the u axis.

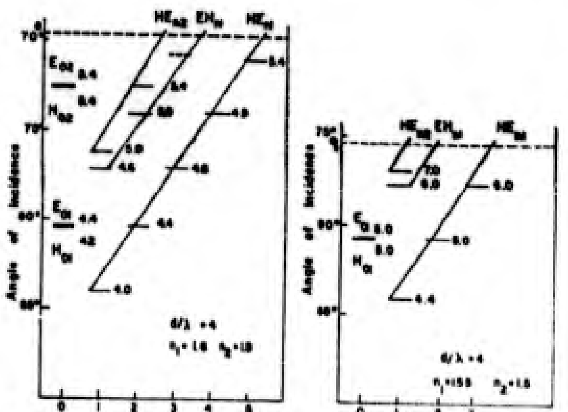

FIG. 3. Chart of solutions to the characteristic Eq. (7). Each bar represents a permissible mode. The m modes for a given n (abscissa) are arranged vertically, each at a height of its corresponding characteristic angle, given by the ordinate. The slanted lines connect modes of the same m number. The number inserted at the right of each bar gives the "optical diameter" of the fiber for that mode. (a) $d/\lambda=4$; $n_1=1.6$ and (b) $d/\lambda=4$; $n_1=1.55$; $n_2=1.5$.

modes, and therefore the number of totally reflected rays decreases. Thus, the parameter R limits the number of permissible characteristic rays in a given fiber. It will thus be an important design parameter of small fiber systems. We will return to this later.

Figure 3 shows a chart of the solution to the characteristic equation for two fibers of the same d/λ, but with different N.A. Each mode is represented by a horizontal bar at its appropriate characteristic angle, given by the ordinate. The m permissible values of characteristic angle for a given n are arranged vertically. The slanted lines connect modes of the same m number. This chart is modeled after the energy-level diagrams of quantum mechanics.

B. Optical Diameter

The numbers given to the right of each bar in Fig. 3 give the "optical diameter" d_0 of the fiber for the corresponding mode. The optical diameter is defined as the diameter of a circular area, perpendicular to the fiber axis and centered on it, through which 99% of the total flux carried in the mode under consideration passes. It is illustrated in Fig. 1(b) and is found by considering the ratio $F(r_0)$, defined by Eq. (10).

$$F(r_0)=\frac{\int_0^{2\pi}\int_0^{r_0}P_z(r,\varphi)rdrd\varphi}{\int_0^{2\pi}\int_0^{\infty}P_z(r,\varphi)rdrd\varphi},\qquad(10)$$

where P is the time-average Poynting vector. Thus r_0 equals $d_0/2$ when $F(r_0)$ equals 0.99. Obviously, d_0 is a measure of the extent of energy penetration into the medium surrounding the fiber core. For practical, image-conveying applications of fiber optics, it is evidently desired that the distance between adjacent fibers be so maintained as not to provide an overlap of their optical diameter.

C. Interference Pattern or Mode Pattern

The interference pattern which may be viewed in the fiber cross section is given mathematically by the time average z component of the Poynting vector. An expression for this for any even wave is given as

$$\begin{aligned}S_z=&(h_{nm}B_{nm}^2/2\omega\mu\cos^2\theta_{nm})\{J_n'^2\cos^2 n\varphi\\&+(n^2J_n^2\sin^2 n\varphi/\beta_{nm}^2r^2)-(1+\sin^2\theta_{nm})\\&\times(nA_{nm}J_nJ_n'/\beta_{nm}r)+A_{nm}^2\sin^2\theta_{nm}[J_n'^2\sin^2 n\varphi\\&+n^2J_n^2\cos^2 n\varphi/\beta_{nm}^2r^2]\},\end{aligned}\qquad(11)$$

where

$$A_{nm}=\left[1-\left(\frac{J_{n+1}(\alpha)}{\alpha J_n(\alpha)}+\frac{K_{n+1}(\gamma)}{\gamma K_n(\gamma)}\right)\Big/\left(\frac{n}{\alpha^2}+\frac{n}{\gamma^2}\right)\right]^{-1}$$

$$\alpha=\frac{\beta_{nm}d}{2},\quad\gamma=\frac{\beta_{nm}'d}{2};$$

as $\theta_{nm}\to\pi/2$, $A_{nm}\to\pm1$,

$$\left.\begin{aligned}EH_{nm}\text{ wave}&\to J_{n+1}^2(\beta_{nm}r)\\HE_{nm}\text{ wave}&\to J_{n-1}^2(\beta_{nm}r)\end{aligned}\right\}.\qquad(12)$$

An expression similar to (11), obtainable by interchange of the $\sin^2(n\phi)$ and $\cos^2 n(\phi)$ terms in that equation, describes the interference pattern of the odd waves. The argument of J_n in (11) is $(\beta_{nm}r)$. J_n' represents the derivative of J_n with respect to this argument.

It may be seen from its definition that the quantity A_{nm} is a constant for a given mode and that the form of the mode pattern depends critically on the value of this constant. For $|A_{nm}|\approx1\approx\sin\theta_{nm}$, the mode patterns display circular symmetry. The HE_{1m} mode has its first maximum on the fiber axis. Between this maximum and the core-coating interface, $m-1$ further maxima and $m-1$ minima appear, each maximum of intensity less than the preceding maximum. For EH_{nm} waves, and for HE_{nm} waves with $n\neq1$, the intensity is zero on the axis. Between the axis and the fiber wall, m maxima, separated by $m-1$ minima, again appear.

The patterns of the H_{om} and E_{om} modes are similar to these, displaying zero intensity on axis and m relative maxima between axis and wall. In order to predict the mode patterns precisely in the general case, Eq. (11) must be evaluated. The first two terms in (11) describe the intensity distribution arising from a pure transverse magnetic wave; the last term describes a pure transverse electric wave. It is seen from Eq. (11) that such distributions are approximated when the absolute value of A is much less or much greater than unity. This condition is approximately satisfied for

(a) (b) (c)

FIG. 4. Photographs of identifiable interference (mode) patterns HE_{13} (a), HE_{41} (b), HE_{12} (c).

modes of intermediate m values in isolated fibers of diameter $\geq 10\lambda$ and large N.A. Experimental evidence indicates that it may be approximated for most modes occurring in fibers in a bundle. This may be explained by the fact that the quantity A_{nm}' is highly sensitive to small changes in eigenvalues. Such changes in the eigenvalues of an isolated fiber are known to be caused by the proximity of other fibers in a bundle.

Even when A_{nm} satisfies this condition, the distributions of intensity in the fiber cross section are difficult to describe generally. A rough description would proceed as follows:

Except for the HE_{1m} modes, the basic pattern of an "nm" mode, as given by the first two terms of (11) in which $\acute{A}_{nm}$ is assumed $\ll 1$, consists of m circles of "maximum" intensity separated by $m-1$ circles of "minimum" intensity, with zero intensity on axis. On each of the circles of "maximum" intensity, which occur approximately at the roots of $J_n(\beta r_{nm})=0$, the intensity varies as $\cos^2 n\phi$, giving rise to $2n$ azimuthal maxima and miñima. On the first of these circles, the intensity is relatively weak. It is strongest on the second, and decreases on succeeding circles.

On the circles of "minimum" intensity, which separate the circles of "maximum" intensity, there occur azimuthal variations according to $\sin^2 n\phi$. With the exception of the first of these circles, the intensity is relatively weak at all azimuths. This is because the amplitude on such circles decreases as $1/r$. On the first circle of "minimum" intensity, however, the maxima which occur at azimuths where $\sin^2 n\phi=1$ are intense, generally much greater than those of the first ring of "maximum" intensity and of the order of those of the second ring of "maximum" intensity. The central photo in Fig. 4, where $m=1$ and $n=4$, illustrates this. Eight maxima at azimuths such that $\sin^2 n\phi=1$ are apparent. The first circle of "maximum" intensity is too weak to be distinguished. The second circle of "maximum" intensity, where the maxima would be $\pi/2$ out of phase with these eight, does not appear, since $m=1$.

For HE_{1m} modes, a similar rough description is applicable, with the exception that the distribution has a maximum on axis, the first "circle" of maximum intensity being coincident with the axis. The first circle of minimum intensity, with $\sin^2 n\phi$ azimuthal variations, merges with the axial maximum, giving rise to distributions such as that in Fig. 4(a), where $m=3$ and $n=1$.

Generally, as A approaches 1, the distributions approach circular symmetry, as illustrated by Fig. 4(c), where $n=1$ and $m=2$. It should be noted that other explanations of the patterns of Fig. 4, with different labeling, are possible, since the value of A_{nm} for fibers in a bundle is not known.

D. Coupled Fibers

Up to this point, the discussion has been confined to the isolated fiber. A rigorous formulation of problems involving close-packed arrays of arbitrary cross-section fibers is considerably complex. Given a *periodic* array of p fibers, of circular cross section, each characteristic angle of the isolated fiber is split into p angles centered about that characteristic angle. With sufficient index difference and separation of fibers, the splitting will be slight. The over-all system will thus have p times as many modes (permissible angles of rays) as the isolated fiber. If only one of these modes is excited in each of the fibers of the bundle, the amplitude and phase must be the same in each fiber. In order to describe a situation in which all the incident energy is limited to one fiber at the entrance end of a bundle, the optical thin-film analog is drawn.

The thin-film analysis will lend considerable insight into the mechanism of energy transfer in a periodic array of fibers. A waveguide mode in an isolated thin film (a slab waveguide) is a combination of one incident and one reflected uniform plane wave, traveling at a discrete angle of incidence θ_m. (See Appendix.) Customary thin-film analysis is entirely adequate in explaining how any combination of such slab waveguides will interact. A stack of p slabs of the same refractive index and thickness, separated by $(p-1)$ films of lesser index, constitutes a periodic array of p slabs. Consider the filter formed by replacing the spacer in a frustrated total reflection filter (Fig. 5) by this stack of p slabs. If instead of the customary T vs λ plot, the transmittance for a given wavelength is plotted as a function of angle of incidence, M transmission bands (in angle) between $\pi/2$ and critical angle will be observed, the mth peak centered on the mth characteristic angle of the

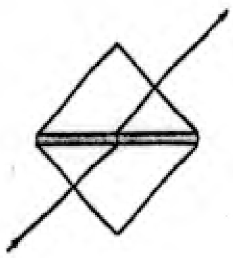

FIG. 5. Illustration of frustrated total reflection and energy coupling in a multilayer, frustrated-total-reflection filter.

isolated slab. This mth band will have p subpeaks occurring at the angles into which the mth characteristic angle of the isolated slab was split due to the proximity of the other slabs. The width of this mth passband is a measure of the tolerances in slab thickness needed to obtain this resonance transmission through the stack. For thick reflecting layers and large index differences, the pass bands are very narrow. Thus, the thin film analysis indicates that high transmittance is possible only if the stack is almost perfectly periodic. (The mathematical development of the foregoing ideas parallels the Kronig-Penney analysis of the periodic, one-dimensional, square well in quantum mechanics.[8])

Another approach to understanding the coupling between a periodic array of slabs may be outlined as follows. A linear combination of the p modes centered about a given mode of the isolated slab may be used to specify the disturbance in the excited slab, with other combinations for other slabs. The process of energy transfer will then be described mathematically by a z-dependent modulation on the amplitude of the disturbance in each slab. Physically, this description depends on the fact that the periodic array has provided a resonance configuration, and energy can be readily transferred.

The present techniques in fabricating fiber bundles do not provide arrays which are sufficiently periodic to satisfy accurately a theory of resonance energy transfer. As a result, a rigorous treatment of energy transfer in a bundle of experimental fibers becomes prohibitively complex. However, from the ray interpretation of energy propagation down a fiber, it is possible to predict roughly the extent of transfer from one fiber to another. The argument proceeds as follows:

In the analysis of a frustrated, total-reflection filter (Fig. 5) one may derive the conditions for resonance transmission from a ray summation method,[2,9] as opposed to the wave equation method thus far employed. In the former method, one considers the amplitude and phase of each ray transmitted through the first low-index film (reflector) into the central high-index film (spacer). At a given point z_0 along the spacer, the intensity is found by adding to the intensity of the directly transmitted ray, the intensities of rays which are transmitted through the reflector into the spacer at other points z less than z_0 and which proceed down the spacer to the point z_0 through multiple reflections at its walls. The intensities of these rays are added with phase information preserved. If all the rays are in phase, or nearly so, that is, if the rays reinforce one another, large intensities occur in the spacer. Otherwise, the intensity in the spacer never becomes much greater than that resulting from a single transmitted ray. The latter may be found from the Fresnel formula for the three-media problems of two high-index prisms separated by a low-index film. The ray-summation method has the advantage that it specifies the intensity as a function of distance from the entrance end of the film and not merely at infinity as given by the wave equation method.

The validity of the ray-summation method in thin-film prediction is unquestioned. Since for coupled circular fibers, only the geometry, not the physics, has changed, a ray-summation method should be valid here. If this is so, however, it is clear that large transfers of energy are not likely to occur between *circular* fibers of reasonable length, since conditions for ray reinforcement can be met precisely for only a single ray, that traveling along the line of centers of two fibers, and this ray carries only a small fraction of the total energy of a mode. Results of experiments to be presented in Sec. V appear to confirm this conclusion.

In view of the foregoing discussion, the following description of the mechanism and extent of energy leakage in a bundle of closely packed fibers, capable of supporting several modes whose optical diameters do not overlap, seems appropriate. We consider a case in which one fiber in such a bundle is illuminated by focusing the image of a white-light source at its entrance end. The fiber accepts part of the incident flux, and various modes in each of many narrow spectral bands are excited and begin to propagate. The flux through the fiber cross section decreases with increasing distance from the entrance end as small fractions of the energy carried in the modes leak by frustrated total reflection to adjacent fibers, forcing them to carry energy at angles other than their natural characteristic angles. (This transfer is insignificant with respect to absorption and would not act to limit the over-all length of the system. Its order of magnitude would be that predicted from Fresnel formula for three-media problems.) Over certain regions of the fiber length, however, a resonance configuration obtains, and a larger transfer of energy occurs because of ray reinforcement (or, equivalently, because of the driving of the natural modes of the adjacent fiber). In a practical fiber system, however, resonant geometry is not maintained for sufficiently long lengths to permit great transfers of energy to occur, except from modes propagating at angles close to the critical angle. At the exit end of the excited fiber, therefore, little or no interference is discernible, since most of the modes have lost little energy and the superposition of all of these for the

[8] R. de L. Kronig and W. G. Penney, Proc. Roy. Soc. (London) A130, 499 (1931).

[9] A. Sommerfeld, *Optics* (Academic Press Inc., New York, 1954), p. 47 ff.

various bands of the spectrum results in a uniform appearance; accordingly, the total flux from this fiber is at least an order of magnitude greater than that of the nearest fibers.

By the same resonance mechanism, the energy in the fibers nearest the excited fiber is transferred to their neighbors. Since almost all of its energy is in modes near critical angle, however, much greater fractions of the total energy of a secondarily excited fiber may be transferred to a third, and then to a fourth, and so on, leading to flux levels of the same order of magnitude in successive fibers removed from the excited fiber. The full extent of energy transfer within a bundle is, of course, dependent on its length. It is possible that, in a long bundle or in one of small numerical aperture, an oscillation of energy in the mode or modes very close to critical angle could be established, expressible in terms of the z-dependent modulation mentioned earlier.

A wavelength-dependent transfer should also be expected, since, in the excited fiber, a greater fraction of the total energy at the red end of the spectrum will be in modes propagating at characteristic angles in the vicinity of the critical angle. The excited fiber should therefore lose a greater percentage of its long-wavelength radiation. Consequently, since less energy at short wavelengths escapes the excited fiber, and, since greater lengths are required for its transfer, a color gradient from the excited fiber to distant fibers should be visible at the exit end of the bundle. This, in fact, is observed.

As the ray-summation method indicates, the length of the fiber bundle is a critical parameter when resonant geometry is prevalent. From calculations based on a stack of slabs, the lower limits for the lengths of bundles may be obtained. Because fibers are resonant only over portions of their length, however, and because energy transfer is less rapid than in the slab case, the lengths of fiber bundles can, no doubt, be many times these lower limits. In order to obtain a better quantitative description of energy transfer in a fiber bundle, the possibility of adapting quantum mechanical perturbation theory to this problem is being investigated. Such an adaptation to the problem of two-fiber coupling has apparently been made,[10] but this work is as yet unreported in the literature.

IV. EXPERIMENTAL

This section describes the experiments conducted in order to verify the conclusions derived from the theory. Mode excitation in an assembly of fibers by the evanescent boundary wave is observed. As discussed earlier, the degree of coupling between close-packed fibers is dependent on the fiber-characteristic term R and the fiber spacing t. This coupling phenomenon sets the lower limit to the fiber diameter in an image-conveying, fiber assembly. In order to evaluate the influence of coupling on the image-transmitting property of fibers, the flux passing through holes of different diameter is measured in the point-spread function of fiber assemblies of different R and t value.

The optical arrangement employed to study coupling between fibers is shown in Fig. 6. The Airy-disk image of a 50-μ pinhole is formed at the entrance pupil of a single fiber using a 90× apochromatic objective of N.A.$=0.95$. The exit end of fibers is viewed with the aid of an oil-immersion microscope of N.A.$=1.2$. Use is made of two small-angle rotatory prisms in between the pinhole and the microscope objective in order to achieve fine image motion. This is necessary in order to excite only a single fiber of micron or submicron dimension. An auxiliary microscope using a beam splitter is made use of in order to view the entrance end of fibers. The wavelength of incident radiation is selected by using a monochromator. The optical arrangement providing means for taking either photomicrographs or photoelectric flux measurements by using a scanning mechanism is also shown.

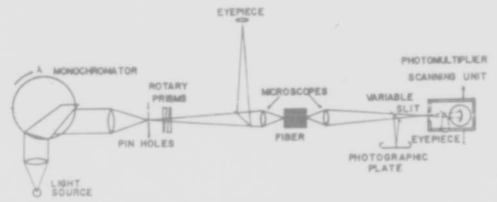

FIG. 6. Optical setup for investigating waveguide effects in isolated fibers and assemblies of fibers.

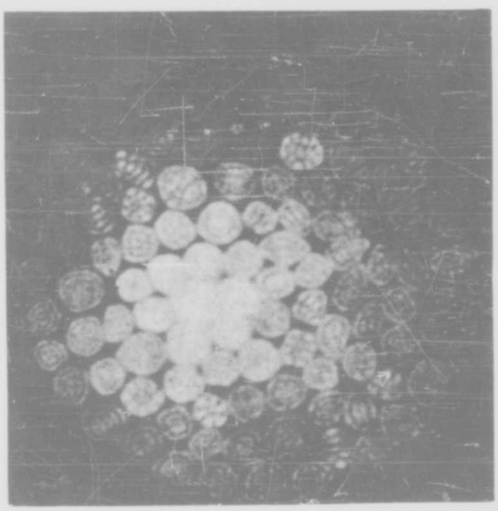

FIG. 7. Typical photomicrograph of exit end of a bundle, illustrating waveguide mode coupling when a single fiber is excited. ($d\approx3\mu$; $n_1=1.61$, $n_2=1.52$.)

[10] E. Snitzer, J. Opt. Soc. Am. 49, 1128(A) (1959).

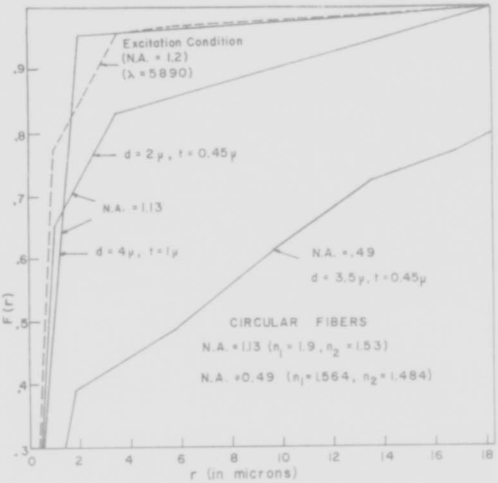

FIG. 8. "Flux passing through a hole" curves for point-spread functions of various fiber assemblies.

A typical photomicrograph of the exit end of fibers, demonstrating the mode excitation due to coupling is shown in Fig. 7. This fiber bundle consists of fibers of approximately 3-μ diameter ($n_1=1.61$, $n_2=1.52$) and it is seen that the excited fiber is capable of propagating a large number of modes and is therefore uniformly illuminated. A color reproduction of Fig. 7 confirmed the theoretical description of energy transfer given in Sec. III(d), i.e., when a fiber in the bundle is excited with white light, the fibers in the immediate vicinity are bluish (for shorter wavelength leakage is less); those farther out show progressive yellow-green and then red predominance. This coupling phenomenon is observed

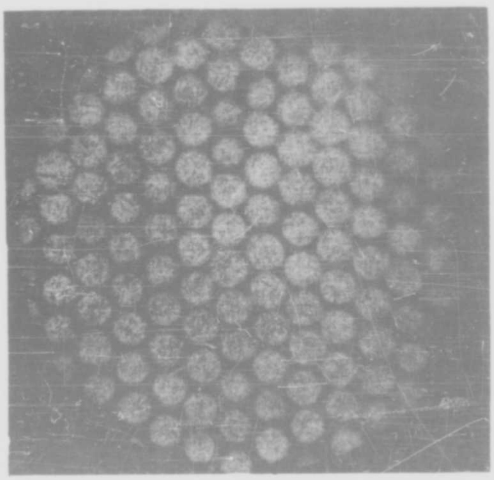

FIG. 9. Photomicrograph of 1.5-μ fiber bundle of N.A. = 1.15.

to be most colorful in fibers of low R value and some interesting mode patterns are observed.

With the same experimental arrangement the average relative flux from an excited fiber (with monochromatic radiation) and the adjacent fibers was determined photoelectrically. The curves of Fig. 8 give the results of such measurements for circular fibers of different diameter and numerical apertures. The amount of flux passing through a hole of variable diameter in the fiber spread function due to coupling is plotted for different fiber bundles. The curve for the incident condition is also included. Figure 9 is a photomicrograph of a portion of a 1.5-μ fiber bundle of N.A. = 1.15 used in this experiment. It is seen that this bundle provided an almost perfectly hexagonal array of nominally circular cross-section fibers. The curves of Fig. 8 are composed of straight lines connecting the experimental points. The first point represents the normalized flux through the excited fiber in the bundle under consideration. The second point gives the flux through the excited fiber plus that through the six fibers surrounding it. One-sixth of the difference between these two measurements provides the average flux from an adjacent fiber. The last point represents the total flux

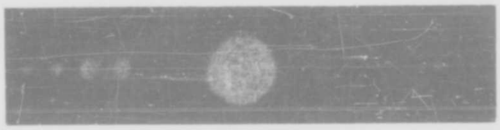

FIG. 10. Photomicrograph of coupling between fibers in a linear array ($d/\lambda=4$; $n_1=1.9$; $n_2=1.5$).

from the bundle. The normalized dashed curve gives the equivalent flux measurements for the exciting radiation. It is seen that the adjacent fibers received some primary excitation due to the inevitable scattering and diffraction in the microscope. The flux from them, therefore is not caused entirely by leakage from the excited fibers.

With the same arrangement, fiber bundles made up of linear arrays of four fibers of different diameters (0.5–5 μ) and spacings were studied. This configuration of fibers obviously lends itself to a somewhat easier interpretation. The relative flux measurements in adjacent fibers were consistent with the plots of Fig. 8. In addition, the effect of the linear configuration on the mode pattern in the fibers adjacent to the excited one may be seen in Fig. 10. This is also seen to be consistent with the theoretical discussion of ray reinforcement on and near the line of centers. The bundles used in these experiments were approximately 0.5 in. long.

From the foregoing discussions and the experimental results presented in Fig. 8, it is evident that the lower limit to the usable fiber diameter for an image-conveying fiber bundle is dependent primarily on the term R and the fiber-spacing t. Whereas light transmission

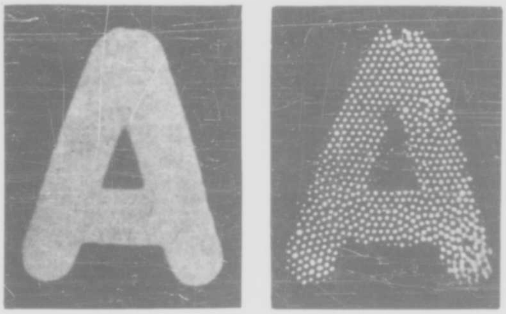

(a) (b)

FIG. 11. Illustrating the imaging capability of a 1-μ fiber bundle (N.A. = 1.15) (a) test object and (b) image of test object.

has been observed in the laboratory in long lengths of isolated fibers less than 0.1 μ in diameter, their optical diameter is considerably larger. Therefore, they are not efficient image transmitters. It has been possible to fabricate aligned fiber bundles of 1-μ-diameter fibers of N.A. 1.15 and they have demonstrated a high degree of optical insulation. Figure 11 shows an image of a test object "A", [Fig. 11(a)] formed by the 1-μ-diameter fiber bundle. A static resolution of 400 lines/mm and dynamic resolution of 800 lines/mm is achieved through these fiber bundles. It is concluded that the lower limit is not yet reached in the laboratory and even higher resolution, fiber bundles are achievable with the availability of higher N.A. fibers.

V. CONCLUSION

In order to describe completely the phenomenon of light conduction in small-diameter fibers, an extension of existing waveguide theory is required. The literature on waveguide theory, though extensive for conducting waveguides, is limited, for dielectric waveguides, to treatments of only a few, lower-order modes. Furthermore, in the optical region where fibers are generally excited with an incoherent polychromatic convergent wave, the problem is even more complex. We have treated the problem from the conventional optical viewpoint of interference and frustrated total reflection. It is seen that the "characteristic waves" or modes are made up of elementary plane waves which are propagated at discrete angles (greater than the critical angle) down the fiber and that these angles are determined by the characteristic equations of the waveguides. Methods for solving these equations are evolved and expressions are derived for the energy distribution inside and outside the fiber. From these the "optical diameter" of fibers is calculated. It is shown that both the number of allowed characteristic angles and the optical diameter are dependent on the "fiber-characteristic term" R which is simply the fiber numerical aperture times its diameter-to-wavelength ratio times π. The larger the value of R, the larger the number of permissible angles and smaller the optical diameter for a given mode.

In order to eliminate significant coupling between fibers in a bundle it is evidently desired that the optical diameters of adjacent fibers do not overlap. For close-packed fibers, substantial coupling occurs and the mode excitation in adjacent fibers is wavelength-dependent. A rigorous formulation of the theory of coupling in experimental fiber assemblies is prohibitively complex. It is nevertheless apparent that considerable insight to the coupling phenomenon may be gained from multilayer, frustrated-total-reflection theory. It is deduced that circular-cross-section fibers are preferable because resonance transfer increases as adjacent fiber surfaces approach a plane parallel configuration. The lower limit to the fiber diameter for an image-conveying system is determined by the term R and the fiber spacing.

This paper also describes experimental techniques for mode excitation by the evanescent boundary wave in an assembly of fibers. Various simple modes and combinations of modes are excited under these conditions and substantial agreement with theory is achieved. A method is developed for measurement of flux passing through a hole through the point spread function of various fiber assemblies. The experimental results indicate that fibers of high numerical aperture down to 1 μ in diameter can yield high image quality. Such fiber bundles have yielded resolutions of 400–800 lines per mm. Whereas long isolated fibers down to 0.1-μ diameter have conducted light, they are not efficient for image transmission because their optical diameter is large. With the availability of higher numerical aperture fibers of circular cross section and development of techniques for fabricating aligned assemblies of them, it seems possible to achieve substantially higher resolution in fiber optics.

APPENDIX. WAVE ANALOGS IN PLANE AND CYLINDRICAL GEOMETRY

The incident and reflected wave interpretation of guided waves in a fiber may be further elucidated through its analog in a slab (a thin-film guide). Consider a thin film of infinite extent in the y and z directions bounded above and below by the planes $x=d$ and $x=0$. Let its index of refraction be n_1 and let it be embedded in an infinite medium of index $n_2<n_1$. We know intuitively that the particular solutions to the wave equation which will satisfy the boundary conditions at plane parallel boundaries are plane waves, incident upon, reflected from, and transmitted through the interface. Let subscripts I, R, and T designate these waves and θ_{1m} and θ_{2m} the angles of incidence and refraction respectively. Since the slab is not infinitely thick, not all angles of incidence, but only certain characteristic angles θ_{1m} yield valid solutions. For the

mth allowed perpendicularly polarized waves we have:

$$\mathbf{E}_{Im} = \hat{y}A_I \exp(ik_1 \cos\theta_{1m}x) \exp(ik_1 \sin\theta_{1m}z - i\omega t)$$
$$\mathbf{E}_{Rm} = \hat{y}A_R \exp(-ik_1 \cos\theta_{1m}x) \exp(ik_1 \sin\theta_{1m}z - i\omega t) \quad \text{(A1)}$$
$$\mathbf{E}_{Tm} = \hat{y}A_T \exp(ik_2 \cos\theta_{2m}x) \exp(ik_2 \sin\theta_{2m}z - i\omega t),$$

where the A's are constant amplitude factors.

If the tangential components of $\mathbf{E}$ and $\mathbf{H}$ are matched at the boundary, a transcendental equation whose roots give the characteristic angles θ_{1m} will result. These angles may also be found from the customary, thin-film approach which determines the conditions of ray reinforcement. For one-half of these angles, it is found that $A_R = -A_I$. We examine these waves further by finding, from the curl relations, the corresponding z components of $\mathbf{H}$. These are given in Eq. (A2).

$$H_{zI} = A_I \frac{k_1 \cos\theta_{1m}}{\omega\mu} \exp(ik_1 \cos\theta_{1m}x) \times \exp(ik_1 \sin\theta_{1m}z - i\omega t)$$

$$H_{zR} = A_I \frac{k_1 \cos\theta_{1m}}{\omega\mu} \exp(-ik_1 \cos\theta_{1m}x) \times \exp(ik_1 \sin\theta_{1m}z - i\omega t) \quad \text{(A2)}$$

$$H_{zT} = A_T \frac{k_2 \cos\theta_{2m}}{\omega\mu} \exp(ik_2 \cos\theta_{2m}x) \times \exp(ik_2 \sin\theta_{2m}z - i\omega t).$$

Snell's law gives

$$k_1 \sin\theta_{1m} = k_2 \sin\theta_{2m} = h_m.$$

To find H_z in medium 1, we merely add H_{zI} and H_{zR}. Thus, for one-half of the characteristic plane waves, the fields are of the form

$$H_{z1m} = A \cos\beta_{1m}x \exp(i\omega t - ih_{1m}z)$$
$$H_{z2m} = B \exp(ik_2 \cos\theta_{2m}x) \exp(i\omega t - ih_m z) \quad \text{(A3)}$$
$$\rightarrow B \exp(-\beta_{2m}x) \exp(i\omega t - ih_m z) \text{ for } \theta_1 > \theta_c.$$

A similar analysis in the cylindrical geometry of fiber leads to Eqs. (A2′) and (A3′).

$$H_{zI} = A_I \frac{k_1 \cos\theta_{10m}}{\omega\mu} H_0^{(1)}(k_1 \cos\theta_{10m}r) \times \exp(ik_1 \sin\theta_{10m}z - i\omega t)$$

$$H_{zR} = A_R \frac{k_1 \cos\theta_{10m}}{\omega\mu} H_0^{(2)}(k_1 \cos\theta_{10m}r) \times \exp(ik_1 \sin\theta_{10m}z - i\omega t) \quad \text{(A}$$

$$H_{zT} = A_T \frac{k_2 \cos\theta_{20m}}{\omega\mu} H_0^{(1)}(k_2 \cos\theta_{20m}r) \times \exp(ik_2 \sin\theta_{20m}z - i\omega t)$$

$$H_{z10m} = H_{zIm} + H_{zRm} = AJ_0(\beta_{10m}r) \exp(i\omega t - ih_{om}z)$$
$$H_{z20m} = BH_0^{(1)}(k_2 \cos\theta_2 r) \exp(i\omega t - ih_{om}z) \quad \text{(A}$$
$$\rightarrow BK_0(\beta_{20m}r) \exp(i\omega t - ih_{om}z) \text{ for } \theta_1 > \theta_{c}$$

where $H_0^{(1)}$ and $H_0^{(2)}$ are the Hankel functions of t first and second kind, respectively. It should be not that (A2′) and (A3′) may be generated from (A and (A3) by the substitutions

$$H_0^{(1)}(k_1 \cos\theta_{10m}r) \rightarrow \exp(ik_1 \cos\theta_1 x)$$
$$H_0^{(2)}(k_1 \cos\theta_{10m}r) \rightarrow \exp(-ik_1 \cos\theta_1 x)$$
$$J_0(\beta_{10m}r) \rightarrow \cos(\beta_{1m}x)$$
$$K_0(\beta_{20m}r) \rightarrow \exp(-\beta_{2m}x).$$

The similarities implied by these substitutions are n accidental, for the asymptotic behavior of the cyli drical functions is, except for a factor $1/(r)^{\frac{1}{2}}$ a constant phase factors, directly proportional to t exponential and trigonometric functions for which th have been substituted. Thus, both physically as incide and reflected waves, and mathematically as form solutions to the wave equation, these functions a the analogs of one another in plane and cylindric geometry.

UNCLASSIFIED

UNCLASSIFIED